EUROPEAN ORGANIZATION FOR NUCLEAR RESEARCH

CERN–PPE/95–30

17 March 1995

Measurements of the τ Polarisation in Z^0 decays

DELPHI Collaboration

Abstract

A sample of $Z^0 \to \tau^+\tau^-$ events observed in the DELPHI detector at LEP in 1991 and 1992 is analysed to measure the τ polarisation in the exclusive decay channels $e\nu\bar{\nu}$, $\mu\nu\bar{\nu}$, $\pi\nu$, $\rho\nu$ and $a_1\nu$. The τ polarisation is also measured with an inclusive hadronic analysis which benefits from a higher efficiency and a better systematic precision than the use of the exclusive decay modes. The results have been combined with those published on the 1990 data. A measurement of the τ polarisation as a function of production angle yields the values for the mean τ polarisation $\langle \mathcal{P}_\tau \rangle = -0.148 \pm 0.022$ and for the Z^0 polarisation $\mathcal{P}_z = -0.136 \pm 0.027$. These results are used to determine the ratio of vector to axial-vector effective couplings for taus $\bar{v}_\tau/\bar{a}_\tau = 0.074 \pm 0.011$ and for electrons $\bar{v}_e/\bar{a}_e = 0.068 \pm 0.014$, compatible with $e-\tau$ universality. With the assumption of lepton universality, the ratio of vector to axial-vector effective couplings for leptons $\bar{v}_l/\bar{a}_l = 0.072 \pm 0.008$ is obtained, implying a value of the effective weak mixing angle $\sin^2\theta^{\rm lept}_{\rm eff} = 0.2320 \pm 0.0021$.

(To be submitted to Zeit. f. Physik C)

P.Abreu[21], W.Adam[50], T.Adye[37], E.Agasi[31], I.Ajinenko[42], R.Aleksan[39], G.D.Alekseev[16], P.P.Allport[22], S.Almehed[24], F.M.L.Almeida[47], S.J.Alvsvaag[4], U.Amaldi[9], S.Amato[47], A.Andreazza[28], M.L.Andrieux[14], P.Antilogus[25], W-D.Apel[17], Y.Arnoud[39], B.Åsman[44], J-E.Augustin[19], A.Augustinus[31], P.Baillon[9], P.Bambade[19], F.Barao[21], R.Barate[14], G.Barbiellini[46], D.Y.Bardin[16], G.J.Barker[35], A.Baroncelli[40], O.Barring[24], J.A.Barrio[26], W.Bartl[50], M.J.Bates[37], M.Battaglia[15], M.Baubillier[23], J.Baudot[39], K-H.Becks[52], M.Begalli[6], P.Beilliere[8], Yu.Belokopytov[9], P.Beltran[11], A.C.Benvenuti[5], M.Berggren[41], D.Bertrand[2], F.Bianchi[45], M.Bigi[45], M.S.Bilenky[16], P.Billoir[23], J.Bjarne[24], D.Bloch[10], M.Blume[52], S.Blyth[35], V.Bocci[38], T.Bolognese[39], M.Bonesini[28], W.Bonivento[28], P.S.L.Booth[22], G.Borisov[42], C.Bosio[40], B.Bostjancic[43], S.Bosworth[35], O.Botner[48], E.Boudinov[42], B.Bouquet[19], C.Bourdarios[9], T.J.V.Bowcock[22], M.Bozzo[13], P.Branchini[40], K.D.Brand[36], R.A.Brenner[15], C.Bricman[2], L.Brillault[23], R.C.A.Brown[9], P.Bruckman[18], J-M.Brunet[8], L.Bugge[33], T.Buran[33], A.Buys[9], M.Caccia[28], M.Calvi[28], A.J.Camacho Rozas[41], T.Camporesi[9], V.Canale[38], M.Canepa[13], K.Cankocak[44], F.Cao[2], F.Carena[9], P.Carrilho[47], L.Carroll[22], C.Caso[13], V.Cassio[45], M.V.Castillo Gimenez[49], A.Cattai[9], F.R.Cavallo[5], L.Cerrito[38], V.Chabaud[9], Ph.Charpentier[9], L.Chaussard[25], J.Chauveau[23], P.Checchia[36], G.A.Chelkov[16], P.Chliapnikov[42], P.Chochula[7], V.Chorowicz[9], V.Cindro[43], P.Collins[9], J.L.Contreras[19], R.Contri[13], E.Cortina[49], G.Cosme[19], F.Cossutti[46], H.B.Crawley[1], D.Crennell[37], G.Crosetti[13], J.Cuevas Maestro[34], S.Czellar[15], E.Dahl-Jensen[29], J.Dahm[52], B.Dalmagne[19], M.Dam[33], G.Damgaard[29], A.Daum[17], P.D.Dauncey[37], M.Davenport[9], W.Da Silva[23], C.Defoix[8], G.Della Ricca[46], P.Delpierre[27], N.Demaria[35], A.De Angelis[9], H.De Boeck[2], W.De Boer[17], S.De Brabandere[2], C.De Clercq[2], C.De La Vaissiere[23], B.De Lotto[46], A.De Min[28], L.De Paula[47], C.De Saint-Jean[39], H.Dijkstra[9], L.Di Ciaccio[38], F.Djama[10], J.Dolbeau[8], M.Donszelmann[9], K.Doroba[51], M.Dracos[10], J.Drees[52], K.-A.Drees[52], M.Dris[32], Y.Dufour[8], F.Dupont[14], D.Edsall[1], R.Ehret[17], G.Eigen[4], T.Ekelof[48], G.Ekspong[44], M.Elsing[52], J-P.Engel[10], N.Ershaidat[23], M.Espirito Santo[21], D.Fassouliotis[32], M.Feindt[9], A.Ferrer[49], T.A.Filippas[32], A.Firestone[1], H.Foeth[9], E.Fokitis[32], F.Fontanelli[13], F.Formenti[9], B.Franek[37], P.Frenkiel[8], D.C.Fries[17], A.G.Frodesen[4], R.Fruhwirth[50], F.Fulda-Quenzer[19], H.Furstenau[9], J.Fuster[49], D.Gamba[45], M.Gandelman[6], C.Garcia[49], J.Garcia[41], C.Gaspar[9], U.Gasparini[36], Ph.Gavillet[9], E.N.Gazis[32], D.Gele[10], J-P.Gerber[10], D.Gillespie[9], R.Gokieli[51], B.Golob[43], G.Gopal[37], L.Gorn[1], M.Gorski[51], V.Gracco[13], F.Grard[2], E.Graziani[40], G.Grosdidier[19], P.Gunnarsson[44], M.Gunther[48], J.Guy[37], U.Haedinger[17], F.Hahn[52], M.Hahn[17], S.Hahn[52], S.Haider[31], Z.Hajduk[18], A.Hakansson[24], A.Hallgren[48], K.Hamacher[52], W.Hao[31], F.J.Harris[35], V.Hedberg[24], R.Henriques[21], J.J.Hernandez[49], P.Herquet[2], H.Herr[9], T.L.Hessing[9], E.Higon[49], H.J.Hilke[9], T.S.Hill[1], S-O.Holmgren[44], P.J.Holt[35], D.Holthuizen[31], M.Houlden[22], J.Hrubec[50], K.Huet[2], K.Hultqvist[44], P.Ioannou[3], J.N.Jackson[22], R.Jacobsson[44], P.Jalocha[18], R.Janik[7], G.Jarlskog[24], P.Jarry[39], B.Jean-Marie[19], E.K.Johansson[44], L.Jonsson[24], C.Joram[9], P.Juillot[10], M.Kaiser[17], G.Kalmus[37], F.Kapusta[23], M.Karlsson[44], E.Karvelas[11], S.Katsanevas[3], E.C.Katsoufis[32], R.Keranen[15], B.A.Khomenko[16], N.N.Khovanski[16], B.King[22], N.J.Kjaer[29], H.Klein[9], A.Klovning[4], P.Kluit[31], J.H.Koehne[17], B.Koene[31], P.Kokkinias[11], M.Koratzinos[9], V.Kostioukhine[42], C.Kourkoumelis[3], O.Kouznetsov[13], P.-H.Kramer[52], M.Krammer[50], C.Kreuter[17], J.Krolikowski[51], I.Kronkvist[24], Z.Krumstein[16], W.Krupinski[18], P.Kubinec[7], W.Kucewicz[18], K.Kurvinen[15], C.Lacasta[49], I.Laktineh[25], S.Lamblot[23], C.Lambropoulos[11], J.W.Lamsa[1], L.Lanceri[46], D.W.Lane[1], P.Langefeld[52], V.Lapin[42], I.Last[22], J-P.Laugier[39], R.Lauhakangas[15], G.Leder[50], F.Ledroit[14], V.Lefebure[2], C.K.Legan[1], R.Leitner[30], Y.Lemoigne[39], J.Lemonne[2], G.Lenzen[52], V.Lepeltier[19], T.Lesiak[36], D.Liko[50], R.Lindner[52], A.Lipniacka[19], I.Lippi[36], B.Loerstad[24], M.Lokajicek[12], J.G.Loken[35], J.M.Lopez[41], A.Lopez-Fernandez[9], M.A.Lopez Aguera[41], D.Loukas[11], P.Lutz[39], L.Lyons[35], J.MacNaughton[50], G.Maehlum[17], A.Maio[21], A.Maltezos[11], V.Malychev[16], F.Mandl[50], J.Marco[41], B.Marechal[47], M.Margoni[36], J-C.Marin[9], C.Mariotti[40], A.Markou[11], T.Maron[52], C.Martinez-Rivero[41], F.Martinez-Vidal[49], S.Marti i Garcia[49], F.Matorras[41], C.Matteuzzi[28], G.Matthiae[38], M.Mazzucato[36], M.Mc Cubbin[9], R.Mc Kay[1], R.Mc Nulty[22], J.Medbo[48], C.Meroni[28], W.T.Meyer[1], A.Miagkov[42], M.Michelotto[36], E.Migliore[45], L.Mirabito[25], W.A.Mitaroff[50], U.Mjoernmark[24], T.Moa[44], R.Moeller[29], K.Moenig[9], M.R.Monge[13], P.Morettini[13], H.Mueller[17], L.M.Mundim[6], W.J.Murray[37], B.Muryn[18], G.Myatt[35], F.Naraghi[14], F.L.Navarria[5], S.Navas[49], P.Negri[28], S.Nemecek[12], W.Neumann[52], N.Neumeister[50], R.Nicolaidou[3], B.S.Nielsen[29], B.Nijjhar[22], V.Nikolaenko[10], P.Niss[44], A.Nomerotski[36], A.Normand[35], W.Oberschulte-Beckmann[17], V.Obraztsov[42], A.G.Olshevski[16], A.Onofre[21], R.Orava[15], K.Osterberg[15], A.Ouraou[39], P.Paganini[19], M.Paganoni[28], P.Pages[10], H.Palka[18], Th.D.Papadopoulou[32], L.Pape[9], F.Parodi[13], A.Passeri[40], M.Pegoraro[36], J.Pennanen[15], L.Peralta[21], H.Pernegger[50], M.Pernicka[50], A.Perrotta[5], C.Petridou[46], A.Petrolini[13], H.T.Phillips[37], G.Piana[13], F.Pierre[39], M.Pimenta[21], S.Plaszczynski[19], O.Podobrin[17], M.E.Pol[6], G.Polok[18], P.Poropat[46], V.Pozdniakov[16], M.Prest[46], P.Privitera[38], A.Pullia[28], D.Radojicic[35], S.Ragazzi[28], H.Rahmani[32], J.Rames[12], P.N.Ratoff[20], A.L.Read[33], M.Reale[52], P.Rebecchi[19], N.G.Redaelli[28], M.Regler[50], D.Reid[9], P.B.Renton[35], L.K.Resvanis[3], F.Richard[19], J.Richardson[22], J.Ridky[12], G.Rinaudo[45], I.Ripp[39], A.Romero[45], I.Roncagliolo[13], P.Ronchese[36], L.Roos[14], E.I.Rosenberg[1], E.Rosso[9], P.Roudeau[19], T.Rovelli[5], W.Ruckstuhl[31], V.Ruhlmann-Kleider[39], A.Ruiz[41], K.Rybicki[18], H.Saarikko[15], Y.Sacquin[39], A.Sadovsky[16], G.Sajot[14], J.Salt[49], J.Sanchez[26], M.Sannino[13], H.Schneider[17], M.A.E.Schyns[52], G.Sciolla[45], F.Scuri[46], Y.Sedykh[16], A.M.Segar[35], A.Seitz[17], R.Sekulin[37], R.C.Shellard[6], I.Siccama[31], P.Siegrist[39], S.Simonetti[39], F.Simonetto[36], A.N.Sisakian[16], B.Sitar[7], T.B.Skaali[33], G.Smadja[25], N.Smirnov[42], O.Smirnova[16], G.R.Smith[37], A.Sokolov[42], R.Sosnowski[51], D.Souza-Santos[6], E.Spiriti[40], S.Squarcia[13], H.Staeck[52], C.Stanescu[40], S.Stapnes[33], I.Stavitski[36], G.Stavropoulos[11], K.Stepaniak[51], F.Stichelbaut[9], A.Stocchi[19], R.Strub[10], B.Stugu[4], M.Szczekowski[51], M.Szeptycka[51], T.Tabarelli[28], J.P.Tavernet[23], O.Tchikilev[42], G.E.Theodosiou[11], A.Tilquin[27],

J.Timmermans[31], L.G.Tkatchev[16], T.Todorov[10], D.Z.Toet[31], A.Tomaradze[2], B.Tome[21], E.Torassa[45], L.Tortora[40], G.Transtromer[24], D.Treille[9], W.Trischuk[9], G.Tristram[8], A.Trombini[19], C.Troncon[28], A.Tsirou[9], M-L.Turluer[39], I.A.Tyapkin[16], M.Tyndel[37], S.Tzamarias[22], B.Ueberschaer[52], S.Ueberschaer[52], O.Ullaland[9], V.Uvarov[42], G.Valenti[5], E.Vallazza[9], C.Vander Velde[2], G.W.Van Apeldoorn[31], P.Van Dam[31], W.K.Van Doninck[2], J.Van Eldik[31], G.Vegni[28], L.Ventura[36], W.Venus[37], F.Verbeure[2], M.Verlato[36], L.S.Vertogradov[16], D.Vilanova[39], P.Vincent[25], L.Vitale[46], E.Vlasov[42], A.S.Vodopyanov[16], M.Voutilainen[15], V.Vrba[12], H.Wahlen[52], C.Walck[44], A.Wehr[52], M.Weierstall[52], P.Weilhammer[9], A.M.Wetherell[9], D.Wicke[52], J.H.Wickens[2], M.Wielers[17], G.R.Wilkinson[35], W.S.C.Williams[35], M.Winter[10], M.Witek[9], G.Wormser[19], K.Woschnagg[48], K.Yip[35], L.Yu[35], O.Yushchenko[42], F.Zach[25], A.Zaitsev[42], A.Zalewska[18], P.Zalewski[51], D.Zavrtanik[43], E.Zevgolatakos[11], N.I.Zimin[16], M.Zito[39], D.Zontar[43], R.Zuberi[35], G.C.Zucchelli[44], G.Zumerle[36]

[1] Ames Laboratory and Department of Physics, Iowa State University, Ames IA 50011, USA
[2] Physics Department, Univ. Instelling Antwerpen, Universiteitsplein 1, B-2610 Wilrijk, Belgium
and IIHE, ULB-VUB, Pleinlaan 2, B-1050 Brussels, Belgium
and Faculté des Sciences, Univ. de l'Etat Mons, Av. Maistriau 19, B-7000 Mons, Belgium
[3] Physics Laboratory, University of Athens, Solonos Str. 104, GR-10680 Athens, Greece
[4] Department of Physics, University of Bergen, Allégaten 55, N-5007 Bergen, Norway
[5] Dipartimento di Fisica, Università di Bologna and INFN, Via Irnerio 46, I-40126 Bologna, Italy
[6] Centro Brasileiro de Pesquisas Físicas, rua Xavier Sigaud 150, RJ-22290 Rio de Janeiro, Brazil
and Depto. de Física, Pont. Univ. Católica, C.P. 38071 RJ-22453 Rio de Janeiro, Brazil
and Inst. de Física, Univ. Estadual do Rio de Janeiro, rua São Francisco Xavier 524, Rio de Janeiro, Brazil
[7] Comenius University, Faculty of Mathematics and Physics, Mlynska Dolina, SK-84215 Bratislava, Slovakia
[8] Collège de France, Lab. de Physique Corpusculaire, IN2P3-CNRS, F-75231 Paris Cedex 05, France
[9] CERN, CH-1211 Geneva 23, Switzerland
[10] Centre de Recherche Nucléaire, IN2P3 - CNRS/ULP - BP20, F-67037 Strasbourg Cedex, France
[11] Institute of Nuclear Physics, N.C.S.R. Demokritos, P.O. Box 60228, GR-15310 Athens, Greece
[12] FZU, Inst. of Physics of the C.A.S. High Energy Physics Division, Na Slovance 2, 180 40, Praha 8, Czech Republic
[13] Dipartimento di Fisica, Università di Genova and INFN, Via Dodecaneso 33, I-16146 Genova, Italy
[14] Institut des Sciences Nucléaires, IN2P3-CNRS, Université de Grenoble 1, F-38026 Grenoble Cedex, France
[15] Research Institute for High Energy Physics, SEFT, P.O. Box 9, FIN-00014 Helsinki, Finland
[16] Joint Institute for Nuclear Research, Dubna, Head Post Office, P.O. Box 79, 101 000 Moscow, Russian Federation
[17] Institut für Experimentelle Kernphysik, Universität Karlsruhe, Postfach 6980, D-76128 Karlsruhe, Germany
[18] High Energy Physics Laboratory, Institute of Nuclear Physics, Ul. Kawiory 26a, PL-30055 Krakow 30, Poland
[19] Université de Paris-Sud, Lab. de l'Accélérateur Linéaire, IN2P3-CNRS, Bat 200, F-91405 Orsay Cedex, France
[20] School of Physics and Materials, University of Lancaster, Lancaster LA1 4YB, UK
[21] LIP, IST, FCUL - Av. Elias Garcia, 14-1°, P-1000 Lisboa Codex, Portugal
[22] Department of Physics, University of Liverpool, P.O. Box 147, Liverpool L69 3BX, UK
[23] LPNHE, IN2P3-CNRS, Universités Paris VI et VII, Tour 33 (RdC), 4 place Jussieu, F-75252 Paris Cedex 05, France
[24] Department of Physics, University of Lund, Sölvegatan 14, S-22363 Lund, Sweden
[25] Université Claude Bernard de Lyon, IPNL, IN2P3-CNRS, F-69622 Villeurbanne Cedex, France
[26] Universidad Complutense, Avda. Complutense s/n, E-28040 Madrid, Spain
[27] Univ. d'Aix - Marseille II - CPP, IN2P3-CNRS, F-13288 Marseille Cedex 09, France
[28] Dipartimento di Fisica, Università di Milano and INFN, Via Celoria 16, I-20133 Milan, Italy
[29] Niels Bohr Institute, Blegdamsvej 17, DK-2100 Copenhagen 0, Denmark
[30] NC, Nuclear Centre of MFF, Charles University, Areal MFF, V Holesovickach 2, 180 00, Praha 8, Czech Republic
[31] NIKHEF-H, Postbus 41882, NL-1009 DB Amsterdam, The Netherlands
[32] National Technical University, Physics Department, Zografou Campus, GR-15773 Athens, Greece
[33] Physics Department, University of Oslo, Blindern, N-1000 Oslo 3, Norway
[34] Dpto. Fisica, Univ. Oviedo, C/P. Pérez Casas, S/N-33006 Oviedo, Spain
[35] Department of Physics, University of Oxford, Keble Road, Oxford OX1 3RH, UK
[36] Dipartimento di Fisica, Università di Padova and INFN, Via Marzolo 8, I-35131 Padua, Italy
[37] Rutherford Appleton Laboratory, Chilton, Didcot OX11 OQX, UK
[38] Dipartimento di Fisica, Università di Roma II and INFN, Tor Vergata, I-00173 Rome, Italy
[39] Centre d'Etude de Saclay, DSM/DAPNIA, F-91191 Gif-sur-Yvette Cedex, France
[40] Istituto Superiore di Sanità, Ist. Naz. di Fisica Nucl. (INFN), Viale Regina Elena 299, I-00161 Rome, Italy
[41] C.E.A.F.M., C.S.I.C. - Univ. Cantabria, Avda. los Castros, S/N-39006 Santander, Spain, (CICYT-AEN93-0832)
[42] Inst. for High Energy Physics, Serpukov P.O. Box 35, Protvino, (Moscow Region), Russian Federation
[43] J. Stefan Institute and Department of Physics, University of Ljubljana, Jamova 39, SI-61000 Ljubljana, Slovenia
[44] Fysikum, Stockholm University, Box 6730, S-113 85 Stockholm, Sweden
[45] Dipartimento di Fisica Sperimentale, Università di Torino and INFN, Via P. Giuria 1, I-10125 Turin, Italy
[46] Dipartimento di Fisica, Università di Trieste and INFN, Via A. Valerio 2, I-34127 Trieste, Italy
and Istituto di Fisica, Università di Udine, I-33100 Udine, Italy
[47] Univ. Federal do Rio de Janeiro, C.P. 68528 Cidade Univ., Ilha do Fundão BR-21945-970 Rio de Janeiro, Brazil
[48] Department of Radiation Sciences, University of Uppsala, P.O. Box 535, S-751 21 Uppsala, Sweden
[49] IFIC, Valencia-CSIC, and D.F.A.M.N., U. de Valencia, Avda. Dr. Moliner 50, E-46100 Burjassot (Valencia), Spain
[50] Institut für Hochenergiephysik, Österr. Akad. d. Wissensch., Nikolsdorfergasse 18, A-1050 Vienna, Austria
[51] Inst. Nuclear Studies and University of Warsaw, Ul. Hoza 69, PL-00681 Warsaw, Poland
[52] Fachbereich Physik, University of Wuppertal, Postfach 100 127, D-42097 Wuppertal 1, Germany

1 Introduction

For the reaction $e^+e^- \to Z^0 \to \tau^+\tau^-$, both the Z^0 and the τ leptons are polarised due to parity violation in the weak neutral current. The polarisation, $\mathcal{P}_\tau$, of the τ leptons can be measured from the τ decay products, assuming the V$-$A structure of the weak charged current, and has, due to the Z^0 polarisation, a dependence on production angle.

At the LEP collider, with a centre-of-mass energy E_{cm} near the Z^0 mass, the production of fermion-antifermion pairs (other than e^+e^-) in e^+e^- annihilation proceeds mainly through s-channel Z^0 exchange. The different strengths of the couplings of the Z^0 to the right-handed and left-handed e^+ and e^- induce a polarisation, $\mathcal{P}_z$, to the produced Z^0. In the absence of beam polarisation, this is given in the improved Born approximation by [1]

$$\mathcal{P}_z = -\frac{2\bar{a}_e\bar{v}_e}{\bar{a}_e^2 + \bar{v}_e^2}, \tag{1}$$

where $\bar{v}_e$ and $\bar{a}_e$ are respectively the vector and axial-vector effective couplings of the electron to the Z^0.

The produced fermions are also polarised due to the different strengths of the couplings of the Z^0 to left and right-handed fermions into which it decays. The mean polarisation $\langle\mathcal{P}_\tau\rangle$ of the τ^- averaged over the full solid angle is

$$\langle\mathcal{P}_\tau\rangle = -\frac{2\bar{a}_\tau\bar{v}_\tau}{\bar{a}_\tau^2 + \bar{v}_\tau^2}, \tag{2}$$

where $\bar{v}_\tau$ and $\bar{a}_\tau$ are respectively the vector and axial-vector effective couplings of the τ to the Z^0. The τ^- and τ^+ are produced with opposite polarisations. Throughout this paper we refer to the polarisation of the τ^-. Due to CP-invariance in charged current leptonic weak decays, the decay products of the τ^+ have the same angular and momentum distributions as their charge conjugate particles in τ^- decays with the opposite polarisation.

The polarisation of the Z^0 induces a dependence of $\mathcal{P}_\tau$ on the polar angle Θ of the τ^- production relative to the incident e^- beam. At the Born level, this has the form

$$\mathcal{P}_\tau(\cos\Theta) = \frac{\langle\mathcal{P}_\tau\rangle\cdot(1+\cos^2\Theta) + \mathcal{P}_z\cdot 2\cos\Theta}{(1+\cos^2\Theta) + \langle\mathcal{P}_\tau\rangle\mathcal{P}_z\cdot 2\cos\Theta}. \tag{3}$$

By studying the dependence of the τ polarisation on Θ the ratios of the effective couplings $\bar{v}_e/\bar{a}_e$ and $\bar{v}_\tau/\bar{a}_\tau$ can be measured simultaneously, allowing a test of e$-\tau$ universality and a comparison with results obtained from forward-backward charge asymmetries. In addition, an estimate of the effective weak mixing parameter for leptons $\sin^2\theta_{\rm eff}^{\rm lept}$ can be derived assuming universality from the relation $\bar{v}_l/\bar{a}_l = 1 - 4\sin^2\theta_{\rm eff}^{\rm lept}$, l =e, τ. This can be compared with results obtained from other measurements to test the validity of the Standard Model.

The above expressions for the polarisations as functions of the vector and axial-vector effective couplings are valid for pure Z^0 exchange at $E_{cm} = M_Z$. The measured polarisations need to be corrected to account for QED effects. They are also slowly varying functions of E_{cm} and corrections need to be applied for data taken with $E_{cm} \neq M_Z$. These corrections are quantified in Section 8 when presenting the combination of the polarisation measurements. They are below the present level of measurement accuracy.

The results given in the following sections are based on a sample of $Z^0 \to \tau^+\tau^-$ events observed in the DELPHI detector in 1991 and 1992 corresponding to an integrated luminosity of 33.6 pb^{-1}. They improve on the analysis of the 1990 data, published in [2],

in both statistical and systematic accuracy. The analysis is confined to the barrel section of the DELPHI detector, the region with polar angle range $|\cos\Theta| < 0.732$. The following exclusive decay channels of the τ have been used as polarimeters:

- $e\nu\bar{\nu}$ using a momentum estimator based on both charged particle momentum and calorimetric energy measurements;
- $\mu\nu\bar{\nu}$ using the μ momentum spectrum;
- $\pi\nu$ and $K\nu$ using the momentum spectrum of the π/K's, where no attempt is made at $\pi-$K separation;
- $\rho\nu$ using the variable ξ described in [3], composed of various decay angles and the ρ invariant mass;
- $a_1\nu$ where the a_1 decays to three charged π's, using moments of various angular distributions sensitive to the τ polarisation [4].

In addition, an inclusive analysis of events where the τ decays to a charged hadron with or without π^0's has been performed. This has a higher efficiency but lower sensitivity per event than the exclusive hadronic analyses. It yields information not already included in the exclusive decays as the event sample is larger and some of the systematic errors have a different origin.

The different techniques used to estimate the τ polarisation are discussed in Section 2. The DELPHI detector is described in Section 3 and its particle identification capabilities in Section 4. The data sample of $e^+e^- \to \tau^+\tau^-$ events used in the analysis is outlined in Section 5. The analyses of the exclusive decay modes and the inclusive hadronic one-prong analysis are described in Sections 6 and 7 respectively. The combination of the results from the different analyses and the results obtained are discussed in Sections 8 and 9.

Discussion of the systematic uncertainty on $\langle \mathcal{P}_\tau \rangle$ for each analysis is contained in the section in which the analysis is described. However, as $\mathcal{P}_z$ is derived from a fit of $\mathcal{P}_\tau$ as a function of the τ production angle $\cos\Theta$, discussion of its systematic uncertainties is postponed to Section 8.

2 Techniques used for τ polarisation determination

The τ polarisation is reflected in the angular distributions of its decay products in the τ rest frame. The angular distribution affects the momenta of the final state particles in the laboratory frame, which can thus be used to infer the τ polarisation.

In the case of a leptonic decay, the only information available to determine the τ polarisation lies in the shape of the momentum spectrum. Ignoring mass effects, at Born level this has the form [1]

$$\frac{1}{N}\frac{dN}{dx} = \frac{1}{3}[(5 - 9x^2 + 4x^3) + \mathcal{P}_\tau(1 - 9x^2 + 8x^3)], \tag{4}$$

where x is the lepton energy divided by the beam energy. The analysis took account of mass effects and higher order corrections.

For a hadronic decay $\tau \to h\nu$ the polar angle θ_h distribution of the hadronic system h with respect to the τ direction as seen in the τ rest frame has the form

$$\frac{1}{N}\frac{dN}{d\cos\theta_h} = \frac{1}{2}(1 + \alpha\mathcal{P}_\tau \cos\theta_h). \tag{5}$$

The angle θ_h can be calculated from the laboratory momentum of the hadronic system p_h via the relation

$$\cos\theta_h \approx \frac{\frac{2p_h}{p_\tau} - 1 - \frac{m_h^2}{m_\tau^2}}{1 - \frac{m_h^2}{m_\tau^2}}, \tag{6}$$

where m_h is the mass of the hadronic system. For a decay containing a spin-0 hadron such as $\pi\nu$ or Kν the constant α is unity. These decays retain the maximum sensitivity to $\mathcal{P}_\tau$.

In decays of the τ to spin-1 particles, the possibility of several polarisation states of the spin-1 particle reduces the sensitivity of the momentum spectrum, the constant α having the form

$$\alpha = \frac{m_\tau^2 - 2m_h^2}{m_\tau^2 + 2m_h^2}. \tag{7}$$

This leads to a sensitivity, relative to that for the $\pi\nu$ decay, of about 0.46 for the $\rho\nu$ and 0.12 for the $a_1\nu$ decay. The sensitivity can be partly regained by including information from the decay of the spin-1 system. The extraction of the τ polarisation will therefore involve a multidimensional distribution, which can be written in the general form

$$W(\vec{x}) = f(\vec{x}) + \mathcal{P}_\tau g(\vec{x}), \tag{8}$$

with $\vec{x}$ representing the set of variables used. These variables are typically functions of the angles between, and the momenta of, the final state particles. It has been shown [3] that no information is lost by using instead the one-dimensional distribution

$$\widehat{W}(\xi) = \hat{f}(\xi)[1 + \mathcal{P}_\tau \xi], \tag{9}$$

where ξ is defined as $\xi = g(\vec{x})/f(\vec{x})$. This approach has been used for the measurement of the τ polarisation in the decays $\tau \to \rho\nu$.

In the inclusive one-prong hadronic analysis discussed in Section 7 the dominant decay channel is $\rho\nu$. The variable used in addition to $\cos\theta_h$ to recuperate the spin information of the hadronic system was related to the angle ψ of the emission of the pions in the ρ rest frame,

$$\cos\psi = \frac{m_h}{\sqrt{m_h^2 - 4m_\pi^2}} \frac{E_{ch} - E_{neu}}{|\vec{p}_{ch} + \vec{p}_{neu}|}, \tag{10}$$

where $E_{ch}, \vec{p}_{ch}$ are the energy and momentum, in the laboratory frame, of the charged pion in the decay and $E_{neu}, \vec{p}_{neu}$ are the energy and momentum of the π^0.

In the one prong decay $\tau \to a_1\nu$, the a_1 decays to $\pi\pi^0\pi^0$ via the intermediate state $\rho\pi^0$. The variable $\cos\psi$ defined in Eq. 10 can also be defined experimentally for the $\tau \to a_1\nu \to \rho\pi^0\nu \to \pi\pi^0\pi^0\nu$ decay by summing over the two π^0's for the neutral energy E_{neu} and momentum $\vec{p}_{neu}$. The ρ carries the spin of the a_1 and although $\cos\psi$ no longer has the strict meaning of Eq. 10, it does retain sensitivity to the polarisation state of the a_1. The 2-dimensional distribution of $\cos\theta_h$ versus $\cos\psi$ for $\tau \to a_1\nu$ has a similar behaviour to that for $\tau \to \rho\nu$, but somewhat smeared. The $\tau \to a_1\nu$ and $\tau \to \rho\nu$ can thus be fitted simultaneously in an inclusive manner in the plane $\cos\theta_h$ versus $\cos\psi$ without significant loss of sensitivity by comparison with the $\tau \to \rho\nu$ channel alone [5].

For the decay $\tau \to a_1\nu \to 3\pi^\pm\nu$ a method has been used which takes advantage of the most complete $\tau \to 3\pi^\pm\nu_\tau$ decay distribution determined in [6]. A fit to various moments of different angles in the 3π system is used. This is discussed in more detail in Section 6.5.

The selected τ decays in each analysis were grouped in six bins of equal width in $\cos\Theta$ between -0.732 and $+0.732$. The polar angle of the decay products is a good

approximation to the τ polar angle, the two angles being typically within 3° of each other. The polarisation $\mathcal{P}_\tau$ in each cosΘ bin for each analysis was then estimated by fitting the data distributions to a linear sum of the predicted distributions for positive and negative polarisation states generated by the KORALZ program [7] using Monte Carlo techniques and passed through a full detector simulation [8]. These distributions included background events. A correction was made for the ratio of the acceptances of the different polarisation states. To determine $\mathcal{P}_z$ and $\langle\mathcal{P}_\tau\rangle$, the polar angle dependence of the τ polarisation was fitted with the function in Eq. 3.

3 The DELPHI detector

The DELPHI detector is described in detail elsewhere [9]. The sub-detector units particularly relevant for this analysis are summarized here. All these covered the full solid angle of the analysis except where specified. In the DELPHI reference frame the z-axis is taken along the direction of the e^- beam. The angle Θ is the polar angle defined with respect to the z-axis and ϕ is the azimuthal angle about this axis. The reconstruction of a charged particle trajectory in the barrel region of DELPHI resulted from a combination of the measurements in:

- the Vertex Detector (VD), made of three layers of 24 cm long single-sided silicon microstrip modules, at radii r of 6.3, 9.0 and 11.0 cm from the beam axis. The space point resolution was about 8 μm and the two track separation was 100 μm in rϕ.
- the Inner Detector (ID), with an inner radius of 12 cm and an outer radius of 28 cm. A jet chamber measured 24 rϕ coordinates and provided track reconstruction. Its two track separation in rϕ was 1 mm and its spatial resolution 50 μm. It was surrounded by an outer part which served mainly for triggering purposes.
- the Time Projection Chamber (TPC), extending from 30 to 122 cm in radius. This was the main detector for the track reconstruction. It provided up to 16 space points for pattern recognition and ionisation information extracted from 192 wires. Every 60° in ϕ there was a boundary region between read-out sectors about 1° wide which had no instrumentation. At cosΘ = 0 there was a cathode plane which caused a reduced tracking efficiency in the polar angle range $|\cos\Theta| < 0.035$. The TPC had a two track separation of about 1.5 cm in rϕ and in z.
- the Outer Detector (OD) with 5 layers of drift cells at a radius of 2 metres from the beam axis. Each layer provided a space point with 110 μm precision in rϕ.

These detectors were surrounded by a solenoidal magnet with a 1.2 Tesla field parallel to the z-axis. In addition to the detectors mentioned above, the identification of the τ decay products relied on:

- the barrel electromagnetic calorimeter, a High density Projection Chamber (HPC). This detector lay immediately outside the tracking detectors and inside the magnet coil. Eighteen radiation lengths deep for perpendicular incidence, its energy resolution was $\Delta E/E = 6.5\%$ for electrons with an energy of 45.6 GeV. It had a high granularity and provided a sampling of shower energies from nine layers in depth. It allowed a determination of the starting point of an electromagnetic shower with an accuracy of 0.003 radians in polar angle and 0.006 radians in azimuthal angle. The HPC had a modularity of 15° in azimuthal angle. Between modules there was a region with a width of about 1° in azimuth where the resolution of electromagnetic showers was degraded. In this region a different treatment of the data had to be carried out for certain analyses.

- the Hadron Calorimeter (HCAL), sensitive to hadronic showers and minimum ionising particles. It was segmented in 4 layers in depth, with a granularity of 3.75° in polar angle and 2.96° in azimuthal angle. Lying outside the magnet solenoid, it had a depth of 110 cm of iron.
- the barrel Muon Chambers (MUB) consisting of two layers of drift chambers, the first one situated after 90 cm of iron and the second outside the hadron calorimeter. The acceptance in polar angle of the outer layer was slightly smaller than the other barrel detectors and covered the range $|\cos\Theta| < 0.602$. The polar angle range $0.602 < |\cos\Theta|$ was covered by the forward Muon Chambers (MUF) in certain azimuthal zones.

The Ring-Imaging Cherenkov detector (RICH), although not used in the present analyses, had an important effect on the performance of the calorimetry as it contained the majority of the material in the DELPHI barrel region. Lying between the TPC and OD in radius, it was 0.6 radiation lengths deep and 0.15 nuclear interaction lengths deep for particles of perpendicular incidence.

The DELPHI trigger was highly efficient for the τ final states, due to the redundancy existing between its different components. From the comparison of the response of independent components, a trigger efficiency of $(99.98 \pm 0.01)\%$ has been derived.

4 Particle identification and energy calibration

In order to minimize the biases and allow an accurate measurement of the polarisation, a clean separation of the final states is required. The detector response was studied extensively by using simulated data as well as various test samples of real data for which the particle identity was unambiguously known. Examples of such test samples are $e^+e^- \to e^+e^-$ events, $e^+e^- \to \mu^+\mu^-$ events, $e^+e^- \to (e^+e^-)e^+e^-$ events and Compton events (scattering of a beam electron on a virtual photon). Test samples could also be produced using the redundancy of the detector for particle identification. An example of such a sample is $\tau \to \pi n\pi^0$, (n>0), selected using tagging of the π^0 from the electromagnetic calorimetry, which could be used to measure the response of the HCAL and muon chambers to charged pions.

4.1 TPC Ionisation Measurement

The energy loss dE/dx of charged particles through ionisation in the TPC, gives separation between electrons and more massive particles, particularly in the momentum range below 15 GeV/c. After the removal of the 20% of wire hits with the largest pulse heights, to remove tails due to delta rays, the resolution obtained on the dE/dx was 6.1% for isolated tracks in τ decays. The pull variable $\Pi^j_{dE/dx}$ for the hypothesis of particle type j (=e, π, μ,K) was defined as

$$\Pi^j_{dE/dx} = \frac{dE/dx|_{meas} - dE/dx|_{exp}(j)}{\sigma(dE/dx)}, \tag{11}$$

where $dE/dx|_{meas}$ is the measured value, $dE/dx|_{exp}(j)$ is the expectation value for a particle of type j (dependent on its momentum), $\sigma(dE/dx)$ is the resolution. Fig. 1 shows the spectra of $\Pi^\pi_{dE/dx}$ for data samples of electrons and hadrons chosen with independent calorimetric cuts. The separation between the means of the pion and electron signals is 3.5 standard deviations at a momentum of 5 GeV/c and 2.0 standard deviations at 15 GeV/c.

4.2 Electromagnetic calorimetry

The HPC electromagnetic calorimeter is used for electron, photon and π^0 identification. For charged particles E_{ass} is the energy of the electromagnetic shower in the HPC associated to the track. This association requires that the shower lie within about 4 cm of the track impact point on the HPC. For electrons E_{ass} should match the measured particle momentum within measurement errors. Muons, which are minimum ionising, deposit on average 200 MeV energy uniformly in depth in the HPC.

For hadrons the value should be lower than for electrons because some hadrons pass through the HPC without interacting and those which do interact in the HPC leave a significant energy deposition only from the decays of π^0's in the interaction products. The ratio of the energy deposition in the HPC to the reconstructed momentum has a peak at one for electrons and a rising distribution towards zero for hadrons. The pull variable $\Pi_{E/p}$ is defined as

$$\Pi_{E/p} = \frac{E_{ass}/p' - 1}{\sigma\left(E_{ass}/p'\right)}, \tag{12}$$

where p' is the reconstructed momentum excluding the OD from the track fit, discussed below in Section 4.5, and $\sigma(E_{ass}/p')$ is the the expected resolution for an electron of momentum p'. $\Pi_{E/p}$ should thus be centered on zero with unit width for electrons and be negative for hadrons and muons. The distribution of $\Pi_{E/p}$ is plotted in Fig. 2 for electrons in τ decays selected using TPC dE/dx and hadrons in τ decays selected using TPC dE/dx in conjunction with the HCAL and muon chambers. There is a good separation above 1 GeV. Separation is best at highest momenta.

Electron rejection with high efficiency for hadron selection can be performed using the associated energy deposition in only the inner four layers of the HPC, corresponding to about six radiation lengths for perpendicular incidence. This is shown in Fig. 3 for both electrons and hadrons.

Photons were identified by electromagnetic showers in the HPC, not associated to charged particles. Hadronic interactions in the HPC could also cause deposition of energy in the HPC which was unassociated with any charged particle. The high granularity of the HPC allowed many such showers to be rejected while retaining electromagnetic showers. An HPC shower which was not associated to a charged particle track was considered to be of electromagnetic origin if it satisfied the following criteria:

- a starting point in the first three layers of the HPC;
- three or more layers of the HPC with deposited energy;
- at least two consecutive layers with deposited energy in the HPC.

These requirements also eliminated some badly measured photon showers near boundary regions in the HPC. Further rejection of hadronic showers was performed by requiring the shower to have an energy greater than 0.5 GeV.

Due to the finite spatial resolution of the electromagnetic calorimeter, the probability for reconstructing a π^0 as either one or two neutral showers was a function of the energy of the π^0. This is illustrated in Fig. 4 which shows the fractions of simulated events with a single π^0 giving zero, one, two and more than two neutral showers in the HPC as functions of the generated π^0 energy. At energies below 2 GeV π^0's appeared mostly as single showers or remained undetected due to the energy threshold in the HPC. At medium energy, between approximately 2 and 10 GeV, most of the π^0's had at least two showers. Above 10 GeV, the two photons tended to be close to one another and were often not resolved in the HPC. The π^0's giving rise to more than two showers were due to photon conversions in front of the HPC and splitting of showers with large fluctuations.

The tail (less than 5%) of π^0's without signals in the HPC was due to photons lost in boundary regions between modules of the HPC.

The energy scale for neutral electromagnetic showers in the HPC was estimated using photons from final state radiative $e^+e^- \to e^+e^-\gamma$ and $e^+e^- \to \mu^+\mu^-\gamma$ events. These photons covered the energy range 5 GeV to 40 GeV. A precision on the neutral energy scale of 2% over the full energy range was estimated.

4.3 Hadron calorimetry and muon identification

A muon candidate appears as a minimum-ionising particle in the hadron calorimeter, penetrating through to the muon chambers. Due to ionisation loss, a momentum of about 2.5 GeV/c was needed in order to penetrate the iron.

Hadron-muon separation was performed with the mean energy deposition per hit layer of the hadron calorimeter E_{hlay}, defined by

$$E_{hlay} = E_{HCAL}/N_{Hlayers}, \tag{13}$$

where E_{HCAL} is the total energy associated to the charged particle in the HCAL and $N_{Hlayers}$ is the number of layers in the HCAL with deposited energy. This is shown in Fig. 5 for pions in $\tau \to \rho\nu \to \pi\pi^0\nu$ events and muons in $e^+e^- \to \mu^+\mu^-$ events. A clean separation between the π and μ signals was obtained by cutting in E_{hlay} around 3 GeV.

One or more hits in the muon chambers, when there was a low energy deposition in the HCAL, gave positive identification of a muon.

4.4 Momentum determination and scale

A good knowledge of the momentum and energy scales is important in the determination of the polarisation. This is particularly true in the leptonic decay channels.

The precision on the momentum component transverse to the beam direction, p_t, obtained with the DELPHI tracking detectors was $\Delta(1/p_t) = 0.0008$ (GeV/c)$^{-1}$ for particles, other than electrons, with the beam momentum. An absolute calibration of the momentum was obtained from $e^+e^- \to \mu^+\mu^-$ events. For lower momenta, more representative of τ decays, the reconstructed momentum was checked from the reconstruction of the masses of the K^0_S and the J/ψ. The absolute momentum scale for particles other than electrons was estimated to be calibrated to a precision of 0.2% over the full momentum range.

4.5 Electron momentum estimation

For the estimation of the momentum of electrons two variables were used. Firstly, for identification purposes, where an estimator from the tracking system was needed, use was made of the reconstructed momentum without inclusion of the information from the OD. Secondly, for the extraction of the τ polarisation from the sample of identified electron candidates, use was made of an estimator based on the combined information from the tracking system and the electromagnetic calorimetry to estimate as accurately as possible the true momentum of the decay electrons.

In passing through the RICH from the TPC to the OD, particles traversed about 60% of a radiation length. Some fraction of electrons would therefore lose substantial energy through bremsstrahlung before reaching the OD. As a consequence, the standard reconstructed momentum of electrons tended to be biased towards lower values. The

effect of radiation could to some extent be circumvented by exclusion of the information from the OD in the reconstruction of electron trajectories. The resulting alternative momentum estimator p' displayed a more Gaussian behaviour for electrons than the standard momentum measurement. It had a resolution of $\Delta(1/p') = 0.002$ (GeV/c)$^{-1}$.

For the extraction of the τ polarisation, a combined momentum estimator was constructed from the measured momentum of the charged particle and the deposited electromagnetic energy. The combination was based on the observation that both the measured momentum p' and the associated electromagnetic energy E_{ass} tended to be biased towards lower values than the true electron momentum. Whereas the momentum bias originated from bremsstrahlung in front of the TPC, the bias on the electromagnetic energy was primarily caused by edge effects in the HPC close to boundary regions between modules. The value of E_{ass}/p' was used to indicate whether p' or E_{ass} was a more reliable estimator for a given electron candidate. This relied on the fact that the downward biases of the two estimators cause opposite effects on the value of E_{ass}/p'. An algorithm was constructed such that, when E_{ass}/p' was consistent with the electron hypothesis, i.e. close to unity, the two estimators p' and E_{ass} were combined through a weighted mean, where the weights were inversely proportional to the square of the measurement uncertainties. However, the further the value of E_{ass}/p' was away from the electron hypothesis, the more the weight of the estimator with the lower value was scaled down relative to the other. In this way the downward bias in the momentum estimation was reduced significantly and the resolution was improved by exploiting all available information. The final electron momentum estimator, p_{el}, was then obtained by adding to this weighted mean the energy of neutral electromagnetic showers situated within 1° of the track plane on the outside of the track curvature, and hence compatible with bremsstrahlung photons.

The calibration of p_{el} was performed with electron samples where the true momentum was known from kinematic constraints. Non-radiative decays of the Z^0 into e^+e^- pairs provided a high statistics calibration of the high end of the momentum spectrum. Radiative $e^+e^- \to e^+e^-\gamma$ events covered the important momentum range between 20 and 35 GeV/c. For the momentum range below 15 GeV/c a test sample of electrons produced by Compton scattering was used where the unobserved electron was assumed to be scattered through a negligible angle, as confirmed by the Monte Carlo event generator TEEGG [10]. From a comparison of the real and simulated data for the three test samples, p_{el} was shown to be calibrated to a precision of 0.6%.

5 Event sample

The data sample corresponded to an integrated luminosity of 33.6 pb^{-1} composed of: 22.9 pb^{-1} at $E_{cm} = 91.2$ GeV in 1992; 6.7 pb^{-1} at $E_{cm} = 91.2$ GeV in 1991; 4.0 pb^{-1} spread across the six centre-of-mass energies $E_{cm} = 88.5$, 89.5, 90.2, 92.0, 93.0 and 93.7 GeV in 1991. Selected according to the criteria outlined below, it consisted of a high purity sample of dileptonic events ($e^+e^- \to e^+e^-$, $\mu^+\mu^-$, $\tau^+\tau^-$) where cosmic rays, $e^+e^- \to q\bar{q}$ and $e^+e^- \to (e^+e^-)X$ two-photon events had been removed. Backgrounds from the e^+e^- and $\mu^+\mu^-$ final states were removed later in a channel specific way in order to minimise biases.

At LEP energies, a $\tau^+\tau^-$ event appears as two highly collimated low multiplicity jets in approximately opposite directions. An event was separated into hemispheres by a plane perpendicular to the event thrust axis, where the thrust was calculated using all charged particles. To be included in the sample, it was required that the highest

momentum charged particle in at least one of the two hemispheres lie in the polar angle region $|\cos\Theta| < 0.732$.

Background from $e^+e^- \to q\bar{q}$ events was reduced by requiring a charged particle multiplicity less than or equal to six, and an isolation angle, defined as the minimum angle between any two charged particles in different hemispheres, greater than 160°.

Cosmic rays and beam-gas events were rejected by requiring that the highest momentum charged particle in each hemisphere have a point of closest approach to the interaction region less than 4.5 cm in z and less than 1.5 cm in the rϕ plane from the centre of the interaction region. It was furthermore required that these particles have a difference in z of their points of closest approach at the interaction region of less than 3 cm. The offset in z of tracks in opposite hemispheres of the TPC was sensitive to the time of passage of a cosmic ray event with respect to the interaction time of the beams. The background left in the selected sample was computed from the data by interpolating the distributions outside the selected regions.

Two-photon events were removed by requiring a total energy in the event greater than 8 GeV and a total event transverse momentum greater than 0.4 GeV/c.

The preceding requirements were used to produce a sample of dileptonic decays of the Z^0 with 87% efficiency for $\tau^+\tau^-$ events within the polar angle fiducial region, calculated from simulated data. Approximately 27000 $\tau^+\tau^-$ events remained after application of all the cuts described above. The background was estimated to consist of 0.8% from $e^+e^- \to q\bar{q}$ events and 0.4% from two-photon events with respect to the $e^+e^- \to \tau^+\tau^-$ events. The cosmic ray contamination was negligible.

Contamination from $e^+e^- \to \mu^+\mu^-$ and $e^+e^- \to e^+e^-$ events was reduced by requiring that the event acollinearity $\theta_{acol} = \cos^{-1}(-\vec{p}_1 \cdot \vec{p}_2/|\vec{p}_1|/|\vec{p}_2|)$ be greater than 0.5°. The variables $\vec{p}_1$ and $\vec{p}_2$ are the momenta of the highest momenta charged particles in hemisphere 1 and 2 respectively. This cut was applied for all except the $\tau \to \pi(\mathrm{K})\nu$ analysis where the $\mu^+\mu^-$ and e^+e^- final states were not significant backgrounds.

For the analyses of $\rho\nu$ and $a_1\nu$ decays, the background from $\mu^+\mu^-$ and e^+e^- final states was reduced further by requiring that $p_{rad} = (|\vec{p}_1|^2 + |\vec{p}_2|^2)^{1/2}$ be less than the beam momentum p_{beam} and that $E_{rad} = (E_1^2 + E_2^2)^{1/2}$ be less than the beam energy E_{beam}. The variables E_1 and E_2 are the total electromagnetic energies deposited in cones of half angle 30° about the momentum vectors $\vec{p}_1$ and $\vec{p}_2$ respectively.

In all analyses, samples of simulated events were used which had been passed through a detailed simulation of the detector response [8] and reconstructed with the same program as the real data. The Monte Carlo event generators used were: KORALZ [7] for $e^+e^- \to \tau^+\tau^-$ events; DYMU3 [11] for $e^+e^- \to \mu^+\mu^-$ events; BABAMC [12] for $e^+e^- \to e^+e^-$ events; JETSET 7.3 [13] for $e^+e^- \to q\bar{q}$ events; Berends-Daverveldt-Kleiss [14] for $e^+e^- \to (e^+e^-)e^+e^-$ events; the generator described in [15] for $e^+e^- \to (e^+e^-)\mu^+\mu^-$ and $e^+e^- \to (e^+e^-)\tau^+\tau^-$ events.

6 Exclusive τ decays

6.1 $\tau \to e\nu\bar{\nu}$

A $\tau \to e\nu\bar{\nu}$ decay has the signature of an isolated charged particle which produces an electromagnetic shower in the HPC. The produced electrons are ultra-relativistic and leave an ionisation deposition in the TPC corresponding to the plateau region above the relativistic rise. Backgrounds from other τ decays arise principally from one-prong hadronic decays where either the hadron interacts early in the HPC or an accompanying

π^0 decay is wrongly associated to the charged particle track. The polarisation was derived from a fit to the spectrum of the electron momentum estimator p_{el} described in Section 4.5.

To be identified as an electron candidate it was required that a hemisphere contain an isolated charged particle track with a momentum measured without the OD, p', greater than $0.01 \times p_{beam}$. To ensure optimal performance of the HPC it was required that the track lie in the polar angle region $0.035 < |\cos\Theta| < 0.707$, and that its extrapolation to the HPC be further than 1° from the centre of an HPC azimuthal boundary region.

As dE/dx played an important role in the selection, it was demanded that the particle track have at least 38 wires with an ionisation measurement in the TPC. This led to a 4.1% loss of tracks around the boundary regions of the TPC sectors which was well described by the simulated data. It was required that the dE/dx measurement be compatible with that of an electron by demanding that the pull $\Pi^{e}_{dE/dx}$ be greater than -2. This significantly reduced the background from hadrons and muons, especially at low momentum, with a very low loss of signal.

The background was reduced further with a logical OR of two independent sets of selection criteria based on the HPC and the TPC dE/dx respectively. This ensured a high identification efficiency over the full momentum range.

- For particles with $p' > 0.05 \times p_{beam}$ the associated HPC energy had to be compatible with the momentum p': it was required that the pull $\Pi_{E/p}$ be greater than -2. This cut had an overall efficiency of 88%.
- It was required that the TPC dE/dx signal lie more than three standard deviations above that expected for a pion: $\Pi^{\pi}_{dE/dx} > 3$. This had an efficiency which varied from 99.5% for the lowest momentum particles to 10% for momenta of about 20 GeV/c. This criterion was applied only to charged particles with $p' < 0.5 \times p_{beam}$, and had an overall efficiency of 36%.

In order to reduce the residual background from hadronic τ decays it was required that the particle have no muon chamber hits and no associated energy in the HCAL beyond the first layer. Furthermore there could be no neutral HPC shower with an energy greater than 4 GeV in a cone of half angle 18° about the track. Neutral showers within 1° in polar angle of the track and hence compatible with a bremsstrahlung photon were not included in this cut.

The identification criteria were studied using test samples of real data. The efficiency in the high momentum region was obtained from a sample of $e^+e^- \to e^+e^-$ events and in the low momentum region from a sample of $e^+e^- \to (e^+e^-)e^+e^-$ events. For intermediate momenta the redundancy between the dE/dx and HPC criteria was exploited to give a precise determination of each of the two. Since the simulation showed that the two criteria were instrumentally uncorrelated, the overall efficiency was computed from the two independent measurements. An identification efficiency of 94% within the angular and momentum acceptance, excluding the loss due to the cut on the number of TPC wires for dE/dx, was derived. As shown in Fig. 6a, the efficiency was constant within 2% over the full electron energy range. Using the redundancy of the dE/dx and HPC identification requirements in a similar manner, the background from other τ decays, primarily the $\tau \to \rho\nu$ channel, was found to be $(2.2 \pm 0.5)\%$

Most $e^+e^- \to e^+e^-$ events were rejected already with the event acollinearity cut $\theta_{acol} > 0.5°$. Remaining Bhabha contamination was reduced using cuts on the hemisphere opposite the identified decay. These cuts were dependent on the value of p_{el}, defined in Section 4.5, of the identified electron. If p_{el} was less than $0.7 \times p_{beam}$ for the identified electron, the total energy in a cone of half-angle 30° about the track had to be less than

$0.8 \times E_{beam}$; for $p_{el} > 0.7 \times p_{beam}$ both the cone energy and the momentum of the highest momentum track in the opposite hemisphere had to be less than $0.7 \times p_{beam}$. The corresponding efficiency is also shown in Fig. 6a. The step at $0.7 \times p_{beam}$ is due to the above selection criteria, and shows a relative efficiency loss of $(3.5 \pm 0.8)\%$ in the high momentum region.

Background from $e^+e^- \to (e^+e^-)e^+e^-$ events was reduced by asking that, in events with only one charged particle in each hemisphere and where both had momentum less than $0.2 \times p_{beam}$, the dE/dx for the opposite hemisphere track be inconsistent with that of an electron. This gave a relative loss of $(4.0 \pm 0.6)\%$ for $p_{el} < 0.2 \times p_{beam}$.

The selection efficiency within the angular acceptance for $\tau \to e\nu\bar{\nu}$ decays after the Bhabha rejection cuts was 87%, with a background of $(2.1 \pm 0.7)\%$ from Bhabha events and $(0.3 \pm 0.1)\%$ from $e^+e^- \to (e^+e^-)e^+e^-$ events. The background from other τ decays was $(2.2 \pm 0.5)\%$. The selected sample consisted of 5417 candidate decays. The p_{el} spectrum summed over all bins in $\cos\Theta$ is shown in Fig. 6b, with the simulated data spectrum for the fitted value of $\langle \mathcal{P}_\tau \rangle$ superimposed. To reduce the effect of the Bhabha background, the polarisation was fitted only over the region $p_{el} < 0.9 \times p_{beam}$. The Bhabha background in this region was $(0.5 \pm 0.2)\%$.

The polarisation $\mathcal{P}_\tau$ was fitted in each of the six bins of $\cos\Theta$ as described in Section 2. The results are shown in Table 1. A fit of Eq. 3 to $\mathcal{P}_\tau$ as a function of $\cos\Theta$ gave a mean τ polarisation of

$$\langle \mathcal{P}_\tau \rangle = -0.148 \pm 0.077,$$

and a Z^0 polarisation of

$$\mathcal{P}_z = -0.209 \pm 0.111,$$

where the errors are statistical only.

The contributions to the systematic error in $\langle \mathcal{P}_\tau \rangle$ included that due to the identification efficiency (0.025), estimated from cross-checking of dE/dx and HPC cuts. The uncertainty from backgrounds, estimated by varying them within their errors, was, for the Bhabha background, 0.020, for the $e^+e^- \to (e^+e^-)e^+e^-$ background, 0.005, and background from other τ decays 0.020. The 0.6% uncertainty in the electron momentum scale gave an uncertainty of 0.050, and the finite simulated data statistics an error of 0.035, resulting in a total systematic error of 0.072.

6.2 $\tau \to \mu\nu\bar{\nu}$

In $\tau \to \mu\nu\bar{\nu}$ decays the τ polarisation was measured using the reconstructed momentum spectrum for the candidate decays, which were identified using techniques described in Section 4.3.

In order to identify such a decay it was required that there be only one charged particle track in a hemisphere and that it be able to penetrate to the outside of the DELPHI magnet iron. Thus the charged particle reconstructed momentum had to be greater than $0.067 \times p_{beam}$ and lie in the polar angle region $0.035 < |\cos\Theta| < 0.732$. To identify the particle positively as a muon it was required that it have an associated hit in the muon chambers or deposited energy in the outer layer of the HCAL. Rejection of τ decays containing a high energy hadron whose showers penetrated deep into the HCAL was performed by demanding that the average energy deposited per layer E_{hlay}, defined in Section 4.3, be less than 3 GeV. Decays containing a hadron associated to a large hadronic shower in the HPC were rejected by the cut $E_{ass} < 3$ GeV, which was very efficient for muons. By demanding that the neutral electromagnetic energy in a cone of

Bin	cosΘ range	$e\nu\bar{\nu}$	$\mu\nu\bar{\nu}$	$\pi\nu$
1	[−0.732,−0.488]	-0.063 ± 0.171	-0.166 ± 0.159	-0.191 ± 0.091
2	[−0.488,−0.244]	$+0.118 \pm 0.169$	-0.040 ± 0.166	-0.104 ± 0.084
3	[−0.244, 0.000]	$+0.044 \pm 0.217$	$+0.109 \pm 0.182$	-0.008 ± 0.095
4	[0.000,+0.244]	-0.583 ± 0.226	$+0.219 \pm 0.181$	-0.281 ± 0.093
5	[+0.244,+0.488]	-0.180 ± 0.174	-0.275 ± 0.175	-0.295 ± 0.082
6	[+0.488,+0.732]	-0.315 ± 0.173	$+0.009 \pm 0.146$	-0.295 ± 0.087
$\langle\mathcal{P}_\tau\rangle$	systematic error	0.063	0.028	0.036

Bin	cosΘ range	$\rho\nu$	$a_1\nu$	inclusive
1	[−0.732,−0.488]	-0.099 ± 0.079	$+0.137 \pm 0.141$	-0.115 ± 0.051
2	[−0.488,−0.244]	-0.037 ± 0.081	-0.110 ± 0.145	$+0.061 \pm 0.055$
3	[−0.244, 0.000]	$+0.080 \pm 0.079$	-0.136 ± 0.141	-0.105 ± 0.055
4	[0.000,+0.244]	$+0.123 \pm 0.077$	-0.100 ± 0.202	-0.165 ± 0.057
5	[+0.244,+0.488]	-0.349 ± 0.083	-0.420 ± 0.162	-0.268 ± 0.048
6	[+0.488,+0.732]	-0.141 ± 0.079	-0.363 ± 0.177	-0.273 ± 0.045
$\langle\mathcal{P}_\tau\rangle$	systematic error	0.027	0.051	0.012

Table 1: τ polarisation values in bins of cosΘ for the $e\nu\bar{\nu}$, $\mu\nu\bar{\nu}$, $\pi\nu$, $\rho\nu$, $a_1\nu$ and inclusive analyses. Errors are statistical only. Also shown is the systematic error, excluding that due to simulated data statistics, for the $\langle\mathcal{P}_\tau\rangle$ result for each channel, taken as fully correlated from bin to bin. The systematic uncertainty due to simulated data statistics in each bin is about 30% of the statistical error.

half-angle 30° about the track be less than 1 GeV, both the contamination from $\tau \to \rho\nu$ events and that from $e^+e^- \to \mu^+\mu^-\gamma$ events were reduced.

The detection efficiency was measured with data and simulated test samples of $\tau \to \mu\nu\bar{\nu}$ events selected with tighter requirements in the muon chambers only and covering the whole momentum spectrum, and with samples of both data and simulated $e^+e^- \to \mu^+\mu^-$ events selected with kinematical cuts. The efficiency of the muon identification in the angular and momentum acceptance was 95%, and its momentum dependence is shown in Fig. 7a. The misidentification efficiency of the HCAL and MUB criteria for background τ decays was checked by a comparison of real and simulated data samples of $\tau \to h\nu n\pi^0$, (n>0), events.

Contamination from cosmic ray events was reduced by requiring that at least one of the highest momentum charged particles in either hemisphere have an impact parameter in the rϕ plane of less than 0.3 cm. In events with a single charged particle in both hemispheres it was further required that the difference in z of the point of closest approach of the two tracks to the interaction region be less than 2 cm.

Background from $\mu^+\mu^-$ events remaining after the event acollinearity cut $\theta_{acol} > 0.5°$ was reduced by demanding that p_{rad}, defined in Section 5, be less than $1.2 \times p_{beam}$. Where the highest momentum particle in the other hemisphere had muon chamber hits or energy deposition in the outer layers of the HCAL it was required that the maximum momentum of any charged particle in the event be less than $0.7 \times p_{beam}$. Any event in which a charged particle passed within 1° in ϕ of a TPC sector boundary and in which any charged particle had a momentum greater than $0.6 \times p_{beam}$ was rejected. This removed some $\mu^+\mu^-$ events with poor momentum reconstruction and poor extrapolation of one of

the tracks to the muon chambers. The resulting momentum dependence of the efficiency is shown in Fig. 7a.

The number of candidate τ decays remaining after these cuts was 6617. The overall efficiency to identify a $\tau \to \mu\nu\bar{\nu}$ decay inside the angular and momentum acceptance was 88%. The background was composed of $(3.4 \pm 0.3)\%$ from other τ decays, $(0.5 \pm 0.1)\%$ from $\mu^+\mu^-$ events, $(0.6 \pm 0.1)\%$ from $e^+e^- \to (e^+e^-)\mu^+\mu^-$ events and $(0.4 \pm 0.1)\%$ from cosmic rays.

The polarisation $\mathcal{P}_\tau$ was fitted in each of the six bins of cosΘ as described in Section 2. The results are shown in Table 1. A fit of Eq. 3 to $\mathcal{P}_\tau$ as a function of cosΘ gave a mean τ polarisation of

$$\langle \mathcal{P}_\tau \rangle = -0.033 \pm 0.068,$$

and a Z^0 polarisation of

$$\mathcal{P}_z = +0.024 \pm 0.099,$$

where the errors are statistical only. The momentum spectrum summed over all bins in cosΘ is shown in Fig. 7b, with the simulated data spectrum for the fitted value of $\langle \mathcal{P}_\tau \rangle$ superimposed. The step at $0.7 \times p_{beam}$ stems from the effect on the $\tau \to \mu\nu\bar{\nu}$ events of the criteria for $\mu^+\mu^-$ rejection and is well controlled with data test samples.

Systematic errors in $\langle \mathcal{P}_\tau \rangle$ included the following contributions: the uncertainty in the muon identification efficiency coming from the statistics of the data samples used in its determination (0.017); the uncertainty in the background contamination of hadronic τ decays due to the finite statistics of the data sample used in its determination (0.003); contamination from $e^+e^- \to \mu^+\mu^-$ events (0.012), $e^+e^- \to (e^+e^-)\mu^+\mu^-$ events (0.005) and cosmic rays (0.001); the effect of the $\mu^+\mu^-$ rejection cuts on the selection efficiency in the high momentum region (0.007); the momentum resolution uncertainty and momentum scale (0.017); the finite simulated data statistics (0.030). This resulted in a total systematic uncertainty of 0.041.

6.3 $\tau \to \pi(K)\nu$

A typical $\pi\nu$ or $K\nu$ decay is characterised by a single isolated charged particle which deposits energy deep in the HPC or in the HCAL. The separation of pions from electrons and muons requires the use of almost all components of the DELPHI detector. An important background arises from $\tau \to \rho\nu \to \pi\pi^0\nu$ decays where the π^0 is not detected, due to threshold effects or dead regions in the calorimeter.

For efficient suppression of muons it was required that the isolated charged particle have a momentum exceeding $0.05 \times p_{beam}$ and lie in the polar angular region $0.035 < |\cos\Theta| < 0.707$. In the region near the transition from the barrel to the end-cap part of the detector the muon chamber and HCAL coverages were incomplete. Regions without muon chambers and with a reduced HCAL coverage were excluded from this study, reducing the efficiency in the polar angular region $|\cos\Theta| > 0.616$ by about a factor two.

The separation of pions from muons relied on the observed signal in the HCAL and muon chambers. Whereas muons penetrate the HCAL as minimum ionizing particles and leave signal in the muon chambers, most pions interact early in the HCAL without reaching the muon chambers. A fraction of pions, however, interact late and are therefore likely to be confused with muons. To reduce this effect, the mean energy per layer deposited in the HCAL, E_{hlay}, was used to group the charged particle tracks into candidate and non-candidate minimum ionizing particles. In the candidate region, $E_{hlay} < 3$ GeV, the ratio of pions to muons was low. As the pions in this region tended to have low momentum and did not penetrate deep into the HCAL, a muon veto was applied by

excluding all particles which were observed in the muon chambers or the outer layer of the HCAL. For $E_{hlay} \geq 3$ GeV the ratio of pions to muons was high and a muon veto was applied by excluding particles only if they were observed in the outer layers of the muon chambers.

For electron rejection it was required that the electromagnetic energy deposited by the charged particle in the first four HPC layers did not exceed 350 MeV, and that the dE/dx did not exceed the expected signal of a pion by more than two standard deviations: $\Pi^{\pi}_{dE/dx} < 2$. Within 0.5° of an azimuthal boundary between HPC modules, where the rejection power of the HPC criterion was poorer, the dE/dx requirement was tightened by asking that $\Pi^{\pi}_{dE/dx}$ be less than one.

A further reduction of the background from electrons and muons was ensured by requiring that the charged particle was either observed in the HCAL or deposited at least 500 MeV in the last five layers of the HPC.

Hadronic τ decays containing π^0's were rejected by insisting that there be no neutral electromagnetic showers in a cone of half angle 18° about the charged pion. These showers had to satisfy the following criteria: the shower had to be separated by at least 1° from the impact point of the charged particle on the HPC surface, had to start within the first four and extend over at least three HPC layers; a minimum energy of 0.8 and 0.5 GeV was required for the 1991 and 1992 data respectively; showers between 1° and 2° from the charged particle impact point had to have a minimum energy of 1.5 GeV.

The identification criteria were studied as far as possible using real data test samples. The efficiencies of the muon and electron rejection criteria were investigated using a sample of charged hadrons from τ decays to $\rho\nu$ and $a_1\nu$ tagged by the presence of a π^0 in the HPC. The misidentification probabilities were obtained from samples of electrons and muons tagged by kinematic constraints or by the use of independent detector components. No suitable test sample was available to study the criteria aimed at rejecting τ decays containing π^0's. Their study thus relied on consistency checks between real and simulated data where the stabilities of the measured τ polarisation and of the branching fraction result were checked against variations in the photon definition criteria. The overall identification efficiency within the angular and momentum acceptance was estimated to be 65%. The efficiency as a function of momentum, obtained from the simulated data with corrections for observed differences in the real data, is shown in Fig. 8a.

The background from $e^+e^- \rightarrow e^+e^-(\gamma)$ and $e^+e^- \rightarrow \mu^+\mu^-(\gamma)$ events was reduced by requirements on the hemisphere opposite to the identified candidate decay. It was asked that the highest momentum charged particle in that hemisphere lie in the polar angle region $0.035 < |\cos\Theta| < 0.732$. Requirements were applied dependent on whether this particle was identified as a muon or electron candidate, using loose criteria. These requirements were different if the momentum of the pion candidate was less than or greater than $0.7 \times p_{beam}$. If it was greater, the track momentum in the opposite hemisphere had to be less than $0.75 \times p_{beam}$. For electron candidates the electromagnetic energy deposited in the hemisphere had to be less than $0.75 \times E_{beam}$, while for muon candidates the sum of these two quantities had to be less than $0.75 \times p_{beam}$. If it was below, the total electromagnetic energy in the opposite hemisphere had to be less than $0.75 \times E_{beam}$ for electron candidates; otherwise the momentum had to be less than $0.85 \times p_{beam}$. These criteria, with an overall efficiency of 93% excluding the fiducial requirement, created a relative drop in the efficiency of $(6.5 \pm 0.8)\%$ for momenta exceeding $0.7 \times p_{beam}$.

A total of 2956 candidate decays were selected. The estimated background from other τ decays was $(11.9 \pm 2.7)\%$, including contributions of 7.2% from the $\rho\nu$ mode and 2.8%

from $\pi K^0_L \nu$ final states of the $K^*(892)\nu$ mode. The background of Z^0 decays into electron or muon pairs was $(0.5 \pm 0.2)\%$. Other backgrounds were negligible.

From a fit of Eq. 3 to the obtained values of $\mathcal{P}_\tau$ in the six bins of $\cos\Theta$, as given in Table 1, a mean τ polarisation of

$$\langle \mathcal{P}_\tau \rangle = -0.199 \pm 0.036$$

and a polarisation of the Z^0

$$\mathcal{P}_z = -0.115 \pm 0.057$$

were obtained. The uncertainties are statistical only. The momentum spectrum of all selected candidates is shown in Fig. 8b with the spectrum of the simulated data for the fitted value of $\langle \mathcal{P}_\tau \rangle$ superimposed.

The uncertainty in $\langle \mathcal{P}_\tau \rangle$ due to the momentum scale was negligible for this channel. The systematic error in $\langle \mathcal{P}_\tau \rangle$ included contributions from the identification efficiency and the background estimates. For the identification efficiency, contributions of 0.015 and 0.019, respectively, from the anti-electron and anti-muon requirements, were caused primarily by the limited statistics of the test samples used for their study. At high momenta the statistics of the pion test sample was severely limited. The uncertainty arising from the separation of the $\pi\nu$ decay mode from hadronic modes with accompanying neutral hadrons was estimated through variations of the photon definition criteria and through a simultaneous variation by 30% of the background rates of $\pi n \pi^0 \nu$ and $\pi K^0_L \nu$. From this study a contribution of 0.026 was estimated. The uncertainty arising from the remaining background of $e^+e^- \to e^+e^-(\gamma)$, $\mu^+\mu^-(\gamma)$ events and from the effect on the signal of the rejection criteria aimed against this background was 0.011. The uncertainty due to radiative corrections to the τ decay process [16] contributed an error of 0.001. Combining these contributions in quadrature with the statistical uncertainty of 0.018 from the limited amount of simulated data, a total systematic uncertainty of 0.041 was obtained.

6.4 $\tau \to \rho\nu$

The τ decay to $\rho\nu$ was selected by requesting an isolated charged particle in the polar angle region $|\cos\Theta| < 0.732$ with an accompanying π^0 candidate. The charged particle had to be incompatible with the electron hypothesis using cuts on $\Pi_{E/p}$ and $\Pi_{dE/dx}$ similar to those outlined in Section 6.1.

Candidate π^0's were subdivided in four different classes:

1. two showers of energy E_1 and E_2 with

   $$2.5 \text{ GeV} < E_1 + E_2 < 10 \text{ GeV},$$

   and an angle greater than 1° between the photons and the charged track. The reconstructed two-photon invariant mass had to lie in the range 0.04 GeV/c^2 to 0.25 GeV/c^2.
2. one shower with energy greater than 5 GeV and more than 1° from the charged track.
3. two showers with

   $$E_1 + E_2 > 10 \text{ GeV}.$$

   In this case the second shower was generally either a hadronic interaction of the charged pion or a secondary associated with the main shower. Only the highest

energy shower was used in the calculation of the ρ invariant mass and an additional cut was applied to reduce contamination:

$$\frac{E_1}{E_1 + E_2} > 0.85.$$

4. two neutrals, including at least one photon which had converted before the TPC, with a reconstructed invariant mass in the range 0.04 GeV/c^2 to 0.25 GeV/c^2. Photons which converted into e^+e^- pairs in the material before the start of the TPC were reconstructed with an efficiency of $(73 \pm 1)\%$ in $\rho\nu$ events using the tracks reconstructed in the TPC.

The $\pi\pi^0$ invariant mass distribution is shown in Fig. 9. To reduce background it was required that the reconstructed ρ invariant mass lie in the range 0.48 GeV/c^2 to 1.20 GeV/c^2. The sample remaining after the cuts contained 5903 τ decays. The selection efficiency inside the angular acceptance was 45%. The remaining background from other τ decays was 15.6% consisting of: $\pi\pi^0\pi^0\nu$ $(10.7\pm0.3)\%$; $\pi n\pi^0\nu$, (n>2) $(2.0\pm0.2)\%$; $K\pi^0\nu$ $(1.8\pm0.2)\%$; $\pi\nu$ $(1.1\pm0.1)\%$. Contamination from $e^+e^- \to e^+e^-(\gamma)$ and $e^+e^- \to \mu^+\mu^-(\gamma)$ events was $(0.6 \pm 0.2)\%$.

The polarisation was estimated using the variable ξ described in Eq. 9. This variable was a function of the decay angle of the ρ in the τ rest frame, of the $\pi^\pm$ in the ρ rest frame and the hadronic invariant mass. The dependence of the efficiency on ξ, estimated from simulation, is displayed in Fig. 10a.

The polarisation $\mathcal{P}_\tau$ was fitted in each of the six bins of cosΘ as described in Section 2. The results are shown in Table 1. A fit of Eq. 3 to $\mathcal{P}_\tau$ as a function of cosΘ gave a mean τ polarisation of

$$\langle \mathcal{P}_\tau \rangle = -0.070 \pm 0.033,$$

and a Z^0 polarisation of

$$\mathcal{P}_z = -0.085 \pm 0.050,$$

where the errors are statistical only. The ξ spectrum summed over all bins in cosΘ is shown in Fig. 10b, with the simulated data spectrum for the fitted value of $\langle \mathcal{P}_\tau \rangle$ superimposed.

The systematic uncertainty in $\langle \mathcal{P}_\tau \rangle$ due to the finite statistics of the simulated data was 0.017. An uncertainty of 0.015 due to the energy cuts for the candidate π^0's in classes 1, 2 and 3 was estimated by varying the cut limits over wide ranges. An uncertainty of 0.001 due to the backgrounds from other τ decays was estimated by varying the values of the τ branching ratios within their errors. Uncertainty of the HPC energy resolution and scale contributed an error of 0.013. Small discrepancies between data and simulation for high energy neutral showers in class 3 events where the HPC pattern recognition reconstructed a false low energy secondary shower nearby gave an uncertainty of 0.007. The uncertainty due to the π^0 mass cuts was estimated by varying the lower and upper cuts on the π^0 mass to be 0.006. Similarly, by varying the cuts on the ρ mass by 0.15 GeV/c^2 the uncertainty due to the acceptance for ρ particles was estimated to be 0.015. By following the same procedure as in Section 6.3 the uncertainty due to radiative corrections was estimated to be 0.001. The uncertainty in the momentum scale had a negligible effect. The total systematic uncertainty was 0.032.

6.5 $\tau \to a_1\nu \to \pi^-\pi^+\pi^\pm\nu$

The decay $\tau \to 3\pi^\pm\nu_\tau$ is characterised by a topology containing three charged particles with no neutral electromagnetic energy present in that hemisphere.

The first requirement in the selection of such events was that the hemisphere contain three charged particles with an absolute value of the sum of their charges equal to unity. The vector sum of their momenta $\vec{P}_{vis}^{3\pi}$ had to lie in the polar angle region $|\cos\Theta|<0.732$ and have a magnitude greater than 10 GeV/c. As the three particles should originate from a τ decay it was required that the invariant mass of the 3π system be less than 2 GeV/c^2.

An important background source was one-prong τ decays with accompanying photons which converted in the material of the detector to produce a e^+e^- pair. Most conversions take place after the microvertex detector which, together with the beam-pipe, accounts for about 2% of a radiation length of material. Most e^+e^- tracks are thus not expected to produce a signal in the microvertex detector. It was demanded that at least two of the three tracks have at least one associated hit in the microvertex detector. To suppress photon conversion background further, a pair finding algorithm was used to reconstruct the interaction point of the photon. If either of the two possible combinations of oppositely charged particles had a difference in polar angle between the two particles of less than 0.3° and a reconstructed vertex more than 2 cm in the rϕ plane from the interaction region the decay was rejected. No attempt was made to identify e^+e^- pairs from Dalitz decays.

Events with three prongs accompanied by photons were rejected. These photons had to satisfy the requirements described in Section 4.2. A photon was assigned to the 3π hemisphere if the angle between the photon and the 3π resultant momentum direction was less than 30°.

A $\tau \to 3\pi n\gamma\nu$ (n>0) decay can also fake a $\tau \to 3\pi^{\pm}\nu_\tau$ event if the photons overlap with the charged particles and are associated to them. To reject these events and suppress photon conversions further, an additional cut was applied, $E_5^{3\pi}/P_{vis}^{3\pi} < 0.2$, where $E_5^{3\pi}$ is the sum of the energy deposited in the first five layers of the HPC and associated to the tracks.

To reduce non-resonant background, it was required that at least one of the two possible $\pi^+\pi^-$ combinations have an invariant mass in the range 0.6 GeV/c^2 $< m_{\pi^+\pi^-} <$ 1.2 GeV/c^2. This cut was asymmetric with respect to the ρ peak because the background should peak in the low mass region, as was the case for the distribution of like sign charged combinations.

These cuts produced a sample of 1830 candidate $a_1\nu$ events. The efficiency within the polar angle acceptance was 40%. The background from other τ decays was estimated to be (5.9 ± 1.8)%, while other backgrounds were negligible. The 3π invariant mass distribution is shown in Fig. 11. A fit to the mass and width of the a_1, in the Kühn and Santamaria model [17], yielded the values $m_{a_1} = 1270 \pm 15$ MeV/c^2 and $\Gamma_{a_1} = 604 \pm 50$ MeV/c^2, in agreement with other studies of τ decays [18,19].

The $\mathcal{P}_\tau$ measurement was performed with a method based on moments of various decay distributions, as advocated by Kühn and Mirkes [6], whose notation is followed below.

The $\tau \to 3\pi^{\pm}\nu_\tau$ decay rate can be written as

$$d\Gamma_{\tau\to\pi\pi\pi\nu_\tau} \propto \sum_X \bar{L}_X W_X d\gamma d\cos\theta_h d\cos\beta dQ^2 ds_1 ds_2, \qquad (14)$$

where θ_h is the angle in the τ rest frame between the τ flight direction and the direction of emission of the hadronic system, β is the angle in the hadronic rest frame between the normal to the 3π decay plane and the direction of the hadrons in the laboratory system, and γ corresponds to a rotation around the normal to the decay plane and determines the orientation of the pions within their production plane. The hadronic structure functions W_X contain the dynamics of the 3π decay and depend in general on the invariant masses

s_1, s_2 of the two $\pi^+\pi^-$ combinations and on Q^2, the invariant mass of the 3π system. The lepton factors $\bar{L}_X$ are functions of the angles θ_h, β and γ. They also depend on $\mathcal{P}_\tau$.

The hadronic structure functions W_X do not factorize in expression (14). Hence, for a given set of $\cos\theta_h$, γ, $\cos\beta$, s_1, s_2, and Q^2, the $W_X(s_1, s_2, Q^2)$ must be calculated in order to perform a fit to the polarisation. In general, the result will depend on the particular model assumed for the hadronic current.

The values of $\mathcal{P}_\tau$ are derived from a combined fit to the $\cos\theta_h$ distribution and the one-dimensional distributions of the following set of moments as a function of $\cos\theta_h$:

$$\langle(3\cos^2\beta - 1)/2\rangle, \quad \langle\cos 2\gamma\rangle, \quad \langle S_{12}\sin 2\gamma\rangle, \quad \langle S_{12}\cos\beta\rangle,$$

where $S_{12} = (s_1 - s_2)/|s_1 - s_2|$ is the sign of the expression $(s_1 - s_2)$. Fits to each of the distributions have been performed, always finding consistent values, thus allowing cross-checks of the fitting procedure. The polarisation $\mathcal{P}_\tau$ was fitted in each of the six bins of cosΘ as described in Section 2. The results are shown in Table 1. A fit of Eq. 3 to $\mathcal{P}_\tau$ as a function of cosΘ gave a mean τ polarisation of

$$\langle\mathcal{P}_\tau\rangle = -0.184 \pm 0.069,$$

and a Z^0 polarisation of

$$\mathcal{P}_z = -0.264 \pm 0.103,$$

where the errors are statistical only. The data for the two most sensitive moments, summed over all cosΘ bins, are shown in Fig. 12.

The method used for measuring $\mathcal{P}_\tau$ relates the various components of the hadronic current. Thus, particular care should be taken in understanding possible biases due to the model dependence of the hadronic structure functions W_X. The effects of changing the Breit-Wigner parameters, of using different theoretical models [17,20,21] and of the possible presence of a scalar contribution have been investigated. From a detailed analysis [4], an estimate for the uncertainty in $\langle\mathcal{P}_\tau\rangle$ arising from the theoretical modelling of a_1 decays of 0.015 was obtained. The uncertainty in $\langle\mathcal{P}_\tau\rangle$ due to the selection efficiency for 3π was estimated to be 0.030 by varying the selection cuts. The cuts in $m_{\pi^+\pi^-}$ were estimated to contribute an error of 0.020 by varying their values by 40 MeV/c^2. The uncertainty due to the acceptance in $\cos\theta_h$ was estimated to be 0.010 and that due to description of the energy thresholds in the HPC to be 0.010. The uncertainty from the momentum scale and resolution contributed an error of 0.030. The uncertainty arising from the simulated data statistics was 0.030. The total systematic uncertainty was 0.059.

7 Inclusive $\tau \to$ one-prong hadronic decay

The highest sensitivity to the τ polarisation is obtained in the decays to $\pi\nu$ and $\rho\nu$. The identification of these channels requires, however, stringent cuts in order to avoid background contamination, mostly due to hadronic decays with more π^0's.

An inclusive measurement was made of the polarisation for decays to a single charged hadron with or without accompanying π^0's. This increased the selection efficiency, at the expense of a somewhat lower sensitivity per event to the polarisation. A charged particle originating directly from the decay of a τ was selected by requesting that it have associated VD hits. It had to lie in the polar angle range $|\cos\Theta| < 0.732$. Additional tracks were permitted provided that these did not have associated VD hits. This ensured that the hemisphere contained only one charged particle arising directly from the decay of the τ, while keeping a high efficiency for retaining events with a photon conversion. Background

from 3-prong and 5-prong τ decays was negligible. Furthermore, the extrapolation of the τ decay track to the HPC had to lie more than 1° away from any azimuthal boundary region of the HPC as the HPC response to electrons near these regions was degraded, rendering electron rejection more difficult.

The analysis was performed as a function of the hadronic invariant mass, m_h, computed from the charged particle track and all neutral electromagnetic showers in a cone of half angle 30° about the track. It was assumed that the charged particle had the mass of a pion and that the particles causing the neutral showers had no mass. The data were separated into three regions of hadronic mass, below 0.3 GeV/c^2, from 0.3 to 0.9 GeV/c^2 and above 0.9 GeV/c^2 but below 1.8 GeV/c^2 $\approx m_\tau$. These regions correspond to the dominating decay being $\pi\nu$, $\rho\nu$ and $a_1\nu$ respectively.

The first stage of electron rejection was performed using the dE/dx of the TPC. It was required that $\Pi^{\pi}_{dE/dx}$ be less than 2. This cut was particularly important in the low momentum region. Additional cuts described below, dependent on the hadronic invariant mass, were performed to reduce the backgrounds further.

- Decays with low hadronic mass were more heavily contaminated by muons and electrons. In the region $m_h < 0.3$ GeV/c^2, the hadron identification criteria were tighter. To reject electrons, it was required that the associated electromagnetic energy deposited in the first 4 layers of the HPC be less than 1 GeV, or that there be associated energy in the HCAL beyond its first layer. The momentum of the single charged particle had to be greater than $0.067 \times p_{beam}$ to ensure that it had sufficient momentum to reach the muon chambers, thus enabling efficient rejection of muon background. Muons were rejected by requiring that E_{hlay} be greater than 4 GeV or, if E_{hlay} was zero or between 0.6 and 4 GeV, there be no hit in the inner layer of the muon chambers. The region $0 < E_{hlay} < 0.6$ GeV contained few pions and was rejected.
- In the two higher mass bins, the background from muons was small enough not to require additional suppression. For $m_h > 0.3$ GeV/c^2, in order to reject electrons it was required that the electromagnetic energy deposited in the first 4 layers of the HPC be less than 5 GeV, or that there be associated energy in the HCAL beyond its first layer.

In order to reduce the contamination from $\mu^+\mu^-$ and e^+e^- events further it was required that the event acollinearity be greater than 0.5°, that there be no particle in the opposite hemisphere with momentum greater than $0.8 \times p_{beam}$ and that E_{rad}, as defined in Section 5, be less than E_{beam}.

The sample remaining after the cuts contained 15092 τ decays, selected with an efficiency of 78% within the angular and momentum acceptances. The background consisted of (4.0 ± 0.4)% from other τ decays and (0.4 ± 0.2)% from non-τ sources. The distribution of the hadronic mass is presented in Fig. 13. The background affects mostly the region of low hadronic mass. Table 2 shows the percentages for the three signal channels, and the backgrounds, in each of the three invariant mass ranges, taken from simulation. The efficiencies for the $\pi\nu$ and $\rho\nu$ channels are higher than for the exclusive analyses where more stringent cuts were made to remove the $\rho\nu$ and $a_1\nu$ decays respectively. Also shown are the different backgrounds to the three mass regions.

The polarisation was estimated using a 2-dimensional fit to the variables $\cos\theta_h$, defined in Section 2, and $\cos\psi_h$, closely related to the emission angle of the charged pion in the

Mass range	Signal channels			Backgrounds		
[GeV/c^2]	$\pi\nu$	$\rho\nu$	$a_1\nu$	$e\nu\bar{\nu}$	$\mu\nu\bar{\nu}$	non-τ
$m_h < 0.3$	83.8 ± 0.5	5.9 ± 0.2	1.1 ± 0.2	1.1 ± 0.1	5.7 ± 0.6	0.5 ± 0.3
$0.3 < m_h < 0.9$	12.1 ± 0.2	55.9 ± 0.3	20.8 ± 0.4	2.1 ± 0.2	1.2 ± 0.1	0.3 ± 0.2
$0.9 < m_h < 1.8$	4.1 ± 0.2	38.2 ± 0.3	78.1 ± 0.4	0.2 ± 0.1	1.1 ± 0.1	0.3 ± 0.2

Table 2: Columns 2, 3 and 4 contain percentage of the events in each range of measured mass, for each of the three main decay modes used in the inclusive hadronic analysis. Other columns show background percentages in each mass range.

hadronic rest frame, as described in Eq. 10. Its precise form is

$$\cos\psi_h = \frac{E_{ch} - E_{neu}}{E_{ch} + E_{neu}}, \tag{15}$$

where E_{ch} is the energy, calculated using the measured momentum, of the charged particle in the decay and E_{neu} is the neutral energy in a cone of half-angle of 30° about the charged particle. In the low mass region a one dimensional fit to $\cos\theta_h$ only was performed as $\cos\psi_h$ has no real significance in this region.

Fits of $\mathcal{P}_\tau$ in the six bins of cosΘ were performed as described in Section 2 for the three invariant mass regions. The results are shown in Table 3.

cosΘ	$\mathcal{P}_\tau$				
bin	$m_h < 0.3$	$0.3 < m_h < 0.9$	$0.9 < m_h < 1.8$	Combined	$\chi^2/n.d.f.$
1	-0.143 ± 0.085	-0.111 ± 0.076	-0.081 ± 0.142	-0.115 ± 0.053	0.2/2
2	-0.013 ± 0.086	$+0.065 \pm 0.086$	$+0.191 \pm 0.166$	$+0.061 \pm 0.057$	1.3/2
3	-0.221 ± 0.093	-0.045 ± 0.087	-0.012 ± 0.142	-0.105 ± 0.057	2.4/2
4	-0.292 ± 0.086	$+0.008 \pm 0.090$	-0.277 ± 0.140	-0.165 ± 0.059	6.5/2
5	-0.331 ± 0.082	-0.240 ± 0.073	-0.277 ± 0.147	-0.268 ± 0.051	0.7/2
6	-0.338 ± 0.077	-0.216 ± 0.071	-0.256 ± 0.141	-0.273 ± 0.048	1.6/2

Table 3: For the inclusive hadronic analysis, $\mathcal{P}_\tau$ in bins of cosΘ for each of the invariant mass ranges. The uncertainties include simulated data statistics. Mass units are GeV/c^2. The last column gives the χ^2 and number of degrees of freedom of the combined result.

The combination of the three mass regions over the six bins in cosΘ gives a χ^2 of 14.5 for 12 degrees of freedom, showing good compatibility. Thus fits of the polarisation to all three mass ranges combined were made in bins of cosΘ. These are shown in Tables 1 and 3. A fit of Eq. 3 to $\mathcal{P}_\tau$ as a function of cosΘ gave for all three m_h bins combined a mean τ polarisation of

$$\langle\mathcal{P}_\tau\rangle = -0.150 \pm 0.021,$$

and a Z^0 polarisation of

$$\mathcal{P}_z = -0.144 \pm 0.032,$$

where the errors are statistical only. The distributions of $\cos\theta_h$ and $\cos\psi_h$, summed over all cosΘ bins, are displayed in Fig. 14, with the simulated data distributions for the fitted value of $\langle\mathcal{P}_\tau\rangle$ superimposed.

The momentum dependent efficiency for hadrons surviving the muon rejection cuts was estimated from a test sample of pions selected using dE/dx and HPC information.

In this manner uncertainties in the polarisation due to the muon rejection cuts and the cut on HCAL energy beyond the first layer were estimated. In an analogous manner test samples of electrons and muons were used to estimate the uncertainty due to background from other τ decays.

The loss of neutral showers in the HPC due to threshold effects and dead space was responsible for an additional uncertainty. The migration of events between the medium and low mass regions was varied by 20% to give an estimate of the effects of lost π^0's in $\rho\nu$ decays or extra interactions of pions in the detector. This gave anti-correlated changes in the lowest and central invariant mass ranges, and thus a partial cancellation in the overall uncertainty. A similar procedure was carried out between the two highest mass bins.

The branching fractions of the $\pi\nu$, $\rho\nu$ and $\pi\pi^0\pi^0\nu$ decay modes of the τ were varied by the uncertainties in the world average values in [19]. This contains corrections to the uncertainties arising from inconsistencies between results from different experiments.

The invariant mass region boundaries were varied by 0.1 GeV/c^2 and the variation in the polarisation taken as a systematic uncertainty coming from the choice of binning.

The neutral definition was tested by changing the requirements outlined in Section 4.2 to include all neutrals regardless of energy, shower extent and starting layer in the HPC.

The uncertainty due to radiative corrections in the τ decay processes was estimated in the manner described in Section 6.3.

A shower from a π^0 or photon could accidentally be associated to the charged particle, causing the variables used in the analysis to be mismeasured. This was studied by adding the full energy associated to the charged track in the HPC into the neutral cone energy in the definitions of $\cos\theta_h$ and $\cos\psi_h$. The change in the measured polarisation was negligible, in the overall fit and in each mass bin.

The uncertainties, separated into their components for each invariant mass region, are listed in Table 4, showing the cancellation of some systematics. The total systematic uncertainty in the combined value of $\langle\mathcal{P}_\tau\rangle$ was 0.017.

	Mass range [GeV/c^2]			Combined
Systematic source	$m_h < 0.3$	$0.3 < m_h < 0.9$	$m_h > 0.9$	$\Delta\langle\mathcal{P}_\tau\rangle$
Simulation statistics	0.018	0.018	0.035	0.012
Muon rejection	0.009	0.000	0.000	0.005
Neutral energy scale	0.000	0.008	0.008	0.005
Migrations	+0.027	−0.030	−0.010	0.005
τ branching ratios	+0.003	−0.004	−0.011	0.004
Mass binning variation	+0.015	−0.023	−0.020	0.004
Non-τ background	+0.008	−0.001	−0.001	0.003
HCAL energy cut	+0.007	−0.002	−0.010	0.003
Neutral definition	+0.010	−0.013	+0.025	0.003
τ decay background	+0.005	−0.001	0.000	0.002
Radiative corrections	0.001	0.001	0.000	0.001
Total	0.040	0.045	0.051	0.017

Table 4: Systematic errors in $\langle\mathcal{P}_\tau\rangle$ for the inclusive hadronic analysis split into the different mass ranges. The signs of the uncertainties in the second and third mass bins show the direction of change relative to a positive change in the lowest mass region. Absence of signs implies no correlation between mass bins.

8 Combination of results

The results of the different exclusive channels and inclusive one-prong hadronic analysis in each of the six bins of $\cos\Theta$ are shown in Table 1. The fitted values of $\langle \mathcal{P}_\tau \rangle$ and $\mathcal{P}_z$ for each of the individual analyses are shown in Table 5.

Channel	$\langle \mathcal{P}_\tau \rangle$	$\mathcal{P}_z$
$\tau \to e\nu\bar{\nu}$	$-0.148 \pm 0.077 \pm 0.072$	$-0.209 \pm 0.111 \pm 0.006$
$\tau \to \mu\nu\bar{\nu}$	$-0.033 \pm 0.068 \pm 0.041$	$+0.024 \pm 0.099 \pm 0.003$
$\tau \to \pi(\mathrm{K})\nu$	$-0.199 \pm 0.036 \pm 0.041$	$-0.115 \pm 0.057 \pm 0.004$
$\tau \to \rho\nu$	$-0.070 \pm 0.033 \pm 0.032$	$-0.085 \pm 0.050 \pm 0.004$
$\tau \to a_1\nu$	$-0.184 \pm 0.069 \pm 0.059$	$-0.264 \pm 0.103 \pm 0.003$
Inclusive	$-0.150 \pm 0.021 \pm 0.017$	$-0.144 \pm 0.032 \pm 0.003$

Table 5: Values of $\langle \mathcal{P}_\tau \rangle$ and $\mathcal{P}_z$ from the fit of $\mathcal{P}_\tau(\cos\Theta)$ for all channels. Uncertainties are statistical followed by systematic. The systematic error in $\mathcal{P}_z$ contains a systematic error of 0.003 common to all channels.

The correlation coefficient of the statistical uncertainties was estimated to be 0.3 between the inclusive and $\pi\nu$ channel and 0.4 between the inclusive and $\rho\nu$ channel from the overlap of events in the different samples. A maximal correlation in the systematic errors of the $\pi\nu$ and inclusive hadronic analysis was assumed, while the correlation between the uncertainties in the $\rho\nu$ and inclusive hadronic analyses was low, arising principally from the HPC energy threshold uncertainties. The final results were insensitive to the correlation coefficients under a variation of ± 0.1.

The results of the different analyses were combined taking into account the correlations in each of the six bins. The results are shown in Table 6 and in Fig. 15. The χ^2 per degree of freedom is 39.2/30, indicating that the different channels gave compatible results. The statistical part of the error has been multiplied by a factor 1.02 to take account of the anticorrelation of the τ^+ and τ^- helicities in an event.

Bin	$\mathcal{P}_\tau$	χ^2/n.d.f.
1	-0.100 ± 0.043	3.2/5
2	-0.002 ± 0.044	4.7/5
3	-0.042 ± 0.046	6.0/5
4	-0.110 ± 0.047	18.0/5
5	-0.287 ± 0.042	1.8/5
6	-0.244 ± 0.040	5.6/5

Table 6: τ polarisation values in bins of $\cos\Theta$ for the combination of all analyses. The errors are statistical only. The final column shows the χ^2 for each bin of the combination.

The combined data were fitted to the functional form of the polarisation given in Eq. 3. In contrast to the case for $\langle \mathcal{P}_\tau \rangle$, $\mathcal{P}_z$ and its associated systematic uncertainty are dependent on the correlations introduced between different bins in $\cos\Theta$. By combining the simulated data distributions for bins of $\cos\Theta$ reflected in $\cos\Theta = 0$, which had identical acceptance effects, the uncertainty in $\mathcal{P}_z$ due to simulation statistics was greatly reduced. Other systematic uncertainties in the polarisation for the different channels affect $\mathcal{P}_z$ if

they are forward-backward asymmetric in a different way for differently charged decay particles. An example is the track curvature in the TPC, which can be offset by detector effects differently for opposite hemispheres, causing different charge-dependent losses in sector boundaries of the TPC for positive and negative z. This, however, was estimated to have negligible effect on $\mathcal{P}_\tau$. An error in the calibration of the Θ measurement for charged particles would lead to an offset in the measurement of $\mathcal{P}_\tau$. An uncertainty on $\mathcal{P}_\tau$ of 0.002 was estimated due to this effect. Similarly the choice of the decay product polar angle rather than that of the τ generates a smearing of the cosΘ distribution for which the fitted value of $\mathcal{P}_\tau$ must be corrected. From simulated data it was estimated that this offset was less than 0.001 and so an uncertainty of 0.001 in $\mathcal{P}_\tau$ was taken. Misidentification of the τ charge from its decay products was estimated to be less than 1%, leading to a systematic uncertainty on $\mathcal{P}_\tau$ of 0.001.

Systematic uncertainties due to simulated data statistics were assumed to have the maximum possible common error between bins reflected about cos$\Theta = 0$, and no correlations between other pairs of bins. The other systematic errors in $\langle \mathcal{P}_\tau \rangle$ were taken as being common to all cosΘ bins for each channel.

The weighted mean value of cosΘ was taken in each bin as the position of the point in the fit. The uncertainty in $\mathcal{P}_\tau$ due to this procedure was estimated to be less than 0.001. The fit gave the results

$$\langle \mathcal{P}_\tau \rangle = -0.136 \pm 0.018 \pm 0.009 \pm 0.011,$$

$$\mathcal{P}_\tau = -0.131 \pm 0.026 \pm 0.001 \pm 0.003.$$

The first error is statistical, the second is due to the simulated data statistics and the third due to all other systematic uncertainties. The best fit function is plotted superimposed on the data in Fig. 15. The χ^2 per degree of freedom is 9.7/4. The correlation between the fitted values of $\langle \mathcal{P}_\tau \rangle$ and $\mathcal{P}_\tau$ was +0.03. A second fit assuming lepton universality gave the result

$$\langle \mathcal{P}_\tau \rangle = \mathcal{P}_\tau = -0.134 \pm 0.014 \pm 0.006 \pm 0.006.$$

The χ^2 was 9.7 for 5 degrees of freedom, and the best fit function is displayed in Fig. 15.

Alternatively, $\langle \mathcal{P}_\tau \rangle$ and $\mathcal{P}_\tau$ can be derived by combining the results from the fit to $\mathcal{P}_\tau(\cos\Theta)$ obtained separately for each channel. This gave essentially identical results to those shown above with a χ^2/n.d.f. of 5.6/5 for the combination of the $\langle \mathcal{P}_\tau \rangle$ results for the different channels and 6.6/5 for the combination of the $\mathcal{P}_\tau$ results.

The observed polarisations $\langle \mathcal{P}_\tau \rangle$ and $\mathcal{P}_\tau$ have to be corrected for QED effects and for the centre-of-mass energies different to $M_{\rm Z}$. These corrections were evaluated with the program ZFITTER [22]. They have the forms $\langle \mathcal{P}_\tau \rangle^{corr} = \alpha_1 \langle \mathcal{P}_\tau \rangle^{obs} + \Delta_1$ and $\mathcal{P}_\tau^{corr} = \alpha_2 \mathcal{P}_\tau^{obs} + \Delta_2$ where $\alpha_{1,2}$ and $\Delta_{1,2}$ are, respectively, multiplicative and additive corrections to the observed polarisations. Their values for this analysis are $\alpha_1 = \alpha_2 = 1.0206$ and $\Delta_1 = \Delta_2 = -0.0020$, in the Minimal Standard Model for $M_{\rm top} = 150$ GeV/c^2 and $M_{\rm Higgs} = 300$ GeV/c^2. The uncertainties arising from varying $M_{\rm top}$ between 91 and 250 GeV/c^2 had a negligible effect.

Application of these corrections resulted in the following values for the mean τ polarisation and the Z^0 polarisation:

$$\langle \mathcal{P}_\tau \rangle = -0.141 \pm 0.018 \pm 0.009 \pm 0.011,$$

$$\mathcal{P}_\tau = -0.136 \pm 0.027 \pm 0.001 \pm 0.003,$$

where the first error is statistical, the second is due to the finite statistics of the simulated data and the third due to all other systematic uncertainties. The corrected result from

the fit assuming universality was

$$\langle \mathcal{P}_\tau \rangle = \mathcal{P}_{\rm z} = -0.139 \pm 0.015 \pm 0.006 \pm 0.006.$$

The analysis [2] on 1990 data yielded the result for the mean τ polarisation $\langle \mathcal{P}_\tau \rangle = -0.24 \pm 0.07$. This is compatible with the results of the current analysis. They have been combined assuming fully correlated systematic errors, to yield a mean τ polarisation

$$\langle \mathcal{P}_\tau \rangle = -0.148 \pm 0.017(\text{stat.}) \pm 0.014(\text{syst.}),$$

and with the assumption of universality,

$$\langle \mathcal{P}_\tau \rangle = \mathcal{P}_{\rm z} = -0.144 \pm 0.014(\text{stat.}) \pm 0.008(\text{syst.}).$$

9 Summary and Conclusions

The polarisation of the τ and its polar angle dependence have been determined through the study of exclusive decay channels and from an inclusive analysis. The different measurements were found to be consistent with each other. The polar angle dependence is displayed in Fig. 15 and in Table 6. The data have been combined with the published 1990 results [2]. The results were

$$\langle \mathcal{P}_\tau \rangle = -0.148 \pm 0.017(\text{stat.}) \pm 0.014(\text{syst.}),$$

$$\mathcal{P}_{\rm z} = -0.136 \pm 0.027(\text{stat.}) \pm 0.003(\text{syst.}).$$

These results yielded for the ratios of the effective weak couplings of the τ and e respectively

$$\bar{v}_\tau/\bar{a}_\tau = 0.074 \pm 0.011,$$

$$\bar{v}_{\rm e}/\bar{a}_{\rm e} = 0.068 \pm 0.014,$$

supporting the hypothesis of lepton universality.

The assumption of lepton universality yielded the result

$$\langle \mathcal{P}_\tau \rangle = \mathcal{P}_{\rm z} = -0.144 \pm 0.015(\text{stat.}) \pm 0.008(\text{syst.}),$$

giving, for the ratio of effective leptonic couplings,

$$\bar{v}_l/\bar{a}_l = 0.072 \pm 0.008,$$

and leading to the result

$$\sin^2\theta^{\rm lept}_{\rm eff} = 0.2320 \pm 0.0021,$$

compatible with the values obtained from previous measurements of the τ polarisation at LEP [23] and from forward-backward charge asymmetries in Z^0 decays [24].

Acknowledgements

We are greatly indebted to our technical collaborators and to the funding agencies for their support in building and operating the DELPHI detector, and to the members of the CERN-SL Division for the excellent performance of the LEP collider.

References

[1] Z Physics at LEP I, edited by G.Altarelli, R.Kleiss and C.Verzegnassi, CERN 89-08 (1989).

[2] DELPHI Collaboration, P.Abreu et al., Z. Phys. **C55** (1992) 555.

[3] M. Davier et. al., Phys. Lett. **B306** (1993) 411.
A. Rougé, Z. Phys. **C48** (1990) 75.

[4] P. Privitera, Study of the decay $\tau \to 3\pi(n\gamma)\nu_\tau$ with the DELPHI detector at LEP, Doctoral thesis, preprint IEKP-KA/93-01, University of Karlsruhe, January 1993;
P. Privitera, Phys. Lett. **B308** (1993) 163.

[5] B. K. Bullock, K. Hagiwara, A. D. Martin, Nucl. Phys. **B395** (1993) 499.

[6] J. H. Kühn, E. Mirkes, Phys. Lett. **B286** (1992) 381;
J. H. Kühn, E. Mirkes, Z. Phys. **C56** (1992) 661.

[7] S.Jadach and Z.Was, Comp. Phys. Com. **36** (1985) 191;
S.Jadach, B.F.L.Ward and Z.Was, Comp. Phys. Com. **66** (1991) 276.

[8] "DELSIM Reference Manual", DELPHI Note 89-68, Sept. 1989, (unpublished).

[9] DELPHI Collaboration, Nucl. Instr. and Meth. **A303** (1991) 233.

[10] D. Karlen, Nucl. Phys. **B289** (1987) 23.

[11] J. E. Campagne and R. Zitoun, Z. Phys. **C43** (1989) 469.

[12] F. A. Berends, W. Hollik and R. Kleiss, Nucl. Phys. **B304** (1988) 712.

[13] T.Sjöstrand, Comp. Phys. Comm. **27** (1982) 243, ibid. **28** (1983) 229;
T.Sjöstrand and M. Bengtsson, Comp. Phys. Comm. **43** (1987) 367;
T.Sjöstrand, "PYTHIA 5.6 JETSET 7.3 Physics and manual", report CERN-TH 6488/92 (1992).

[14] F.A.Berends, P.H.Daverveldt, R.Kleiss, Phys. Lett. **B148** (1984) 489;
Comp. Phys. Comm. **40** (1986) 271.

[15] T. Todorov, "Détermination des paramètres du modèle standard et tests de sa validité dans les désintegrations hadroniques du Z^0", Doctoral thesis, CRN Strasbourg, report CRN/HE 94-21, 1994.

[16] The LEP collaborations, "Combined Preliminary Data on Z Parameters from the LEP Experiments and Constraints on the Standard Model", report CERN/PPE/94-187, Nov 1994;
R. Decker and F. Finkemeier, Phys. Rev. **D48** (1993) 4203;
M. Finkemeier, "Radiative Corrections to the decay $\tau \to \pi\nu$", Doctoral thesis, University of Karlsruhe, February 1994.

[17] J. H. Kühn, A. Santamaria, Z. Phys. **C48** (1990) 445.

[18] ARGUS Collab., H. Albrecht et al., Z. Phys. **C58** (1993) 61.

[19] Particle Data Group, M.Aguilar-Benitez et al., Phys. Rev. **D50**, (1994) 1173.

[20] N. Isgur, C. Morningstar, C. Reader, Phys. Rev. **D39** (1989) 1357.

[21] M. Feindt, Z. Phys. **C48** (1990) 681.

[22] D. Bardin et al., Z. Phys. **C44** (1989) 493;
D. Bardin et al., "ZFITTER: An Analytical Program for Fermion Pair Production in e^+e^- Annihilation", CERN-TH 6443/92 (1992).

[23] ALEPH Collaboration, D. Decamp et al., Phys. Lett. **B265** (1991) 430;
OPAL Collaboration, G. Alexander et al., Phys. Lett. **B266** (1991) 201;
L3 Collaboration, O. Adriani et al., Phys. Lett. **B294** (1992) 466;
ALEPH Collaboration, D. Buskulic et al., Z. Phys. **C59** (1993) 369;
L3 Collaboration, O. Adriani et al., Phys. Lett. **B341** (1994) 245;
OPAL Collaboration, R. Akers et al., Z. Phys. **C65** (1995) 1.

[24] ALEPH Collaboration, D. Buskulic et al., Z. Phys. **C60** (1993) 71;
ALEPH Collaboration, D. Buskulic et al., Z. Phys. **C62** (1994) 539;
DELPHI Collaboration, P. Abreu et al., Nucl. Phys. **B417** (1994) 3;
DELPHI Collaboration, P. Abreu et al., Nucl. Phys. **B418** (1994) 403;
L3 Collaboration, O. Adriani et al., Phys. Lett. **B307** (1993) 451;
L3 Collaboration, O. Adriani et al., Z. Phys. **C62** (1994) 551;
OPAL Collaboration, P. Acton et al., Z. Phys. **C58** (1993) 219;
OPAL Collaboration, P. Akers et al., Z. Phys. **C61** (1994) 19.

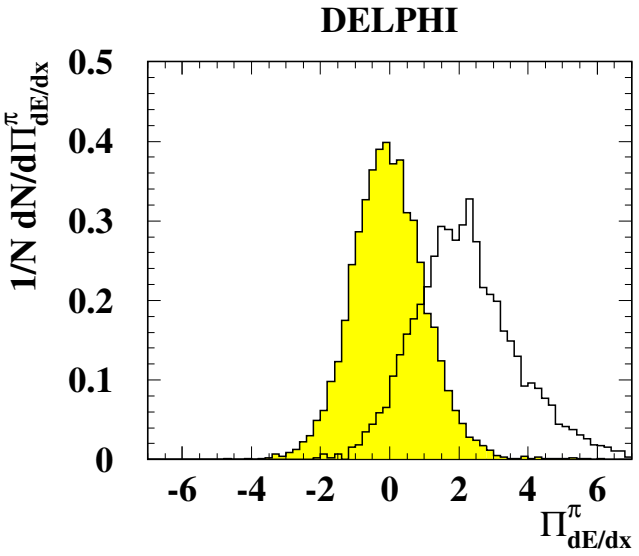

Figure 1: Distribution of the pull on dE/dx for the pion hypothesis, $\Pi^{\pi}_{dE/dx}$, for two different data sets in τ decays. The clear histogram is for an electron test sample. The hatched area shows a pion test sample.

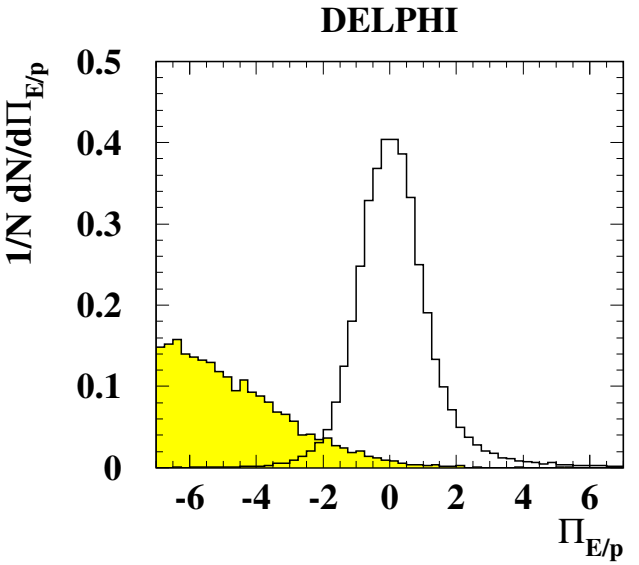

Figure 2: Distributions of the electron identification variable $\Pi_{E/p}$ for samples of electrons (clear histogram) and for pions (hatched histogram). Only particles depositing more than 1 GeV in the HPC were included.

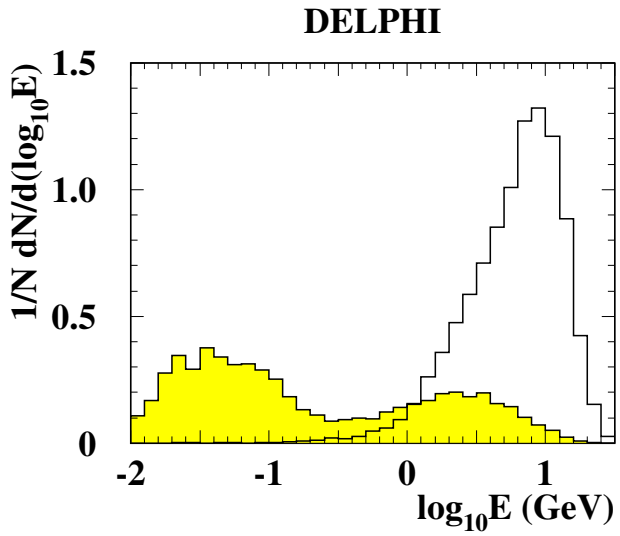

Figure 3: Distribution in data of energy deposition in the first four layers of the HPC for an electron test sample (clear histogram) and a pion test sample (hatched histogram). The area in the hatched histogram is 0.58 as 42% of hadrons did not leave any energy deposition in the first four layers of the HPC. The bump on the right hand side for the hadron sample arises from hadrons which interact in the first four layers of the HPC or in the RICH.

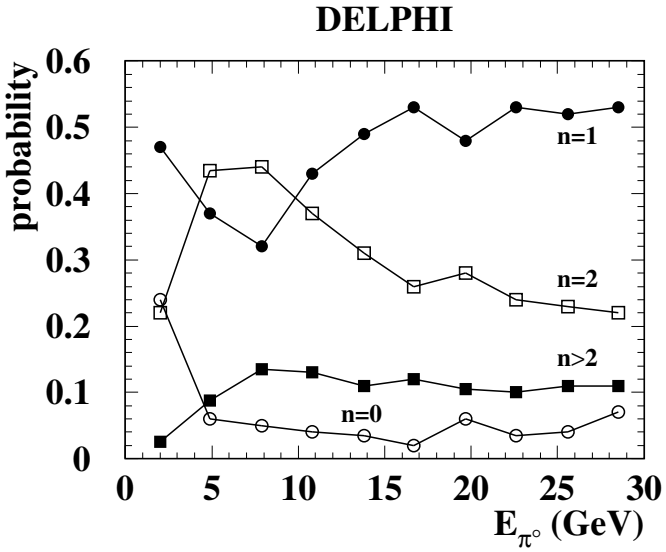

Figure 4: Probabilities of reconstructing a single π^0 in simulated data as n clusters in the HPC as a function of π^0 energy. Open circles are for $n = 0$, solid circles for $n = 1$, open squares for $n = 2$ and solid squares for $n > 2$.

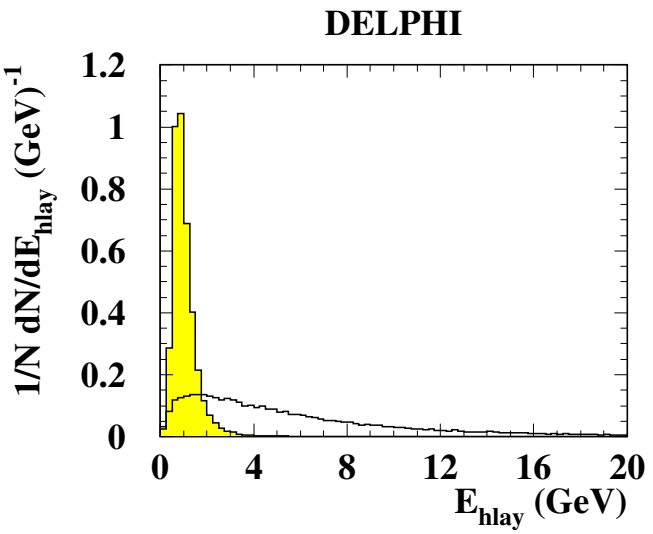

Figure 5: Distribution of average energy per layer E_{hlay} in the hadron calorimeter for real data test samples of pions (clear histogram) and of muons (hatched histogram).

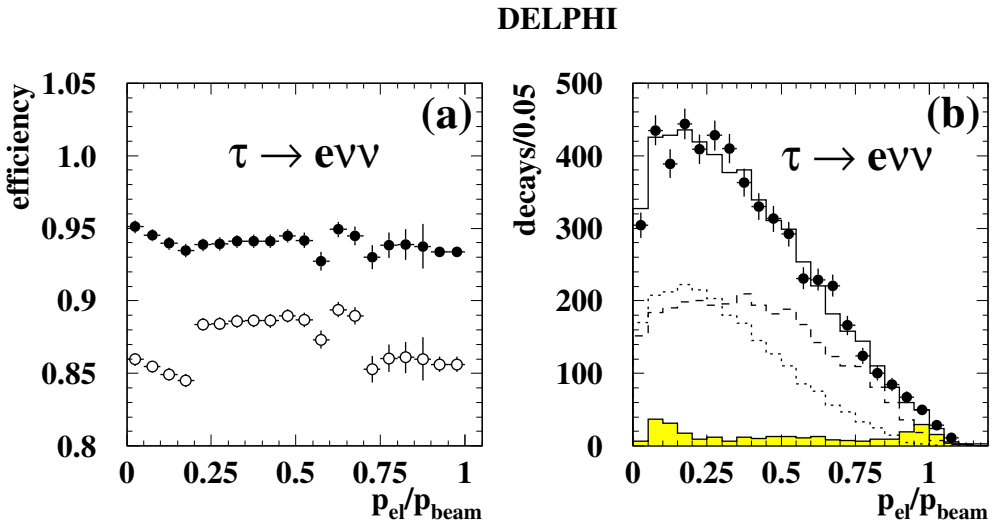

Figure 6: a) The solid circles show the identification efficiency for $\tau \to e\nu\bar{\nu}$ decays as a function of p_{el}/p_{beam}. The open circles show the efficiency after all cuts including rejection of backgrounds other than from τ decays. b) p_{el}/p_{beam} spectrum for candidate $\tau \to e\nu\bar{\nu}$ decays. The dots are data and the solid line is simulated data for the fitted value of $\langle \mathcal{P}_\tau \rangle$. The hatched area is background and the dotted and dashed lines correspond to the positive and the negative polarisation contributions respectively.

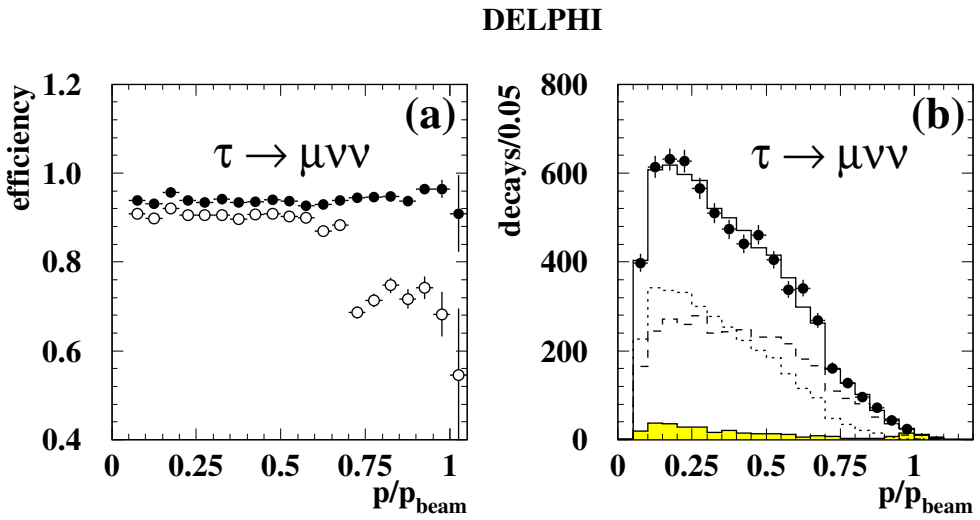

Figure 7: a) The identification efficiency for $\tau \to \mu\nu\bar{\nu}$ decays and b) the spectrum of candidate $\tau \to \mu\nu\bar{\nu}$ decays, as a function of the reconstructed muon momentum normalised to the beam momentum, with the same conventions as in Fig. 6.

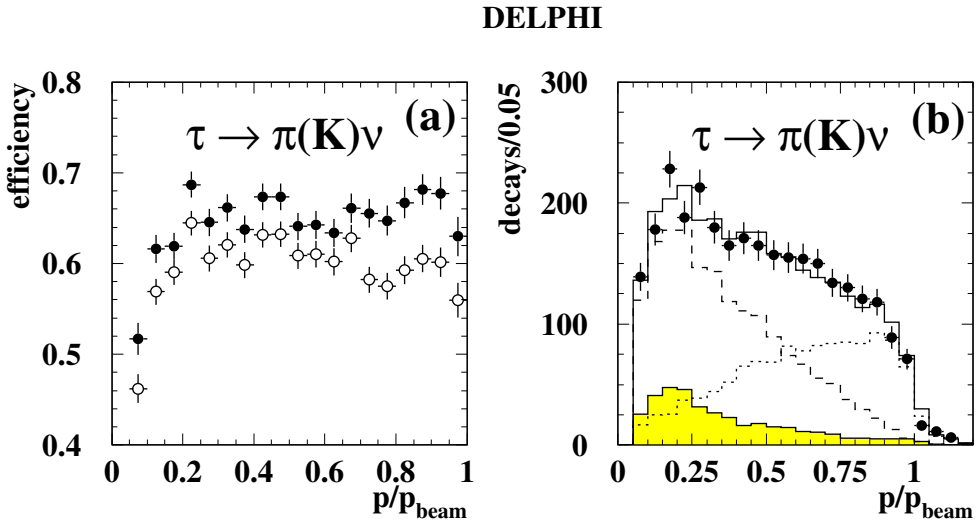

Figure 8: a) The efficiency of identification criteria and b) the spectrum, for $\tau \to \pi(\mathrm{K})\nu$ decays as a function of the $\pi(\mathrm{K})$ momentum normalised to the beam momentum, with the same conventions as in Fig. 6.

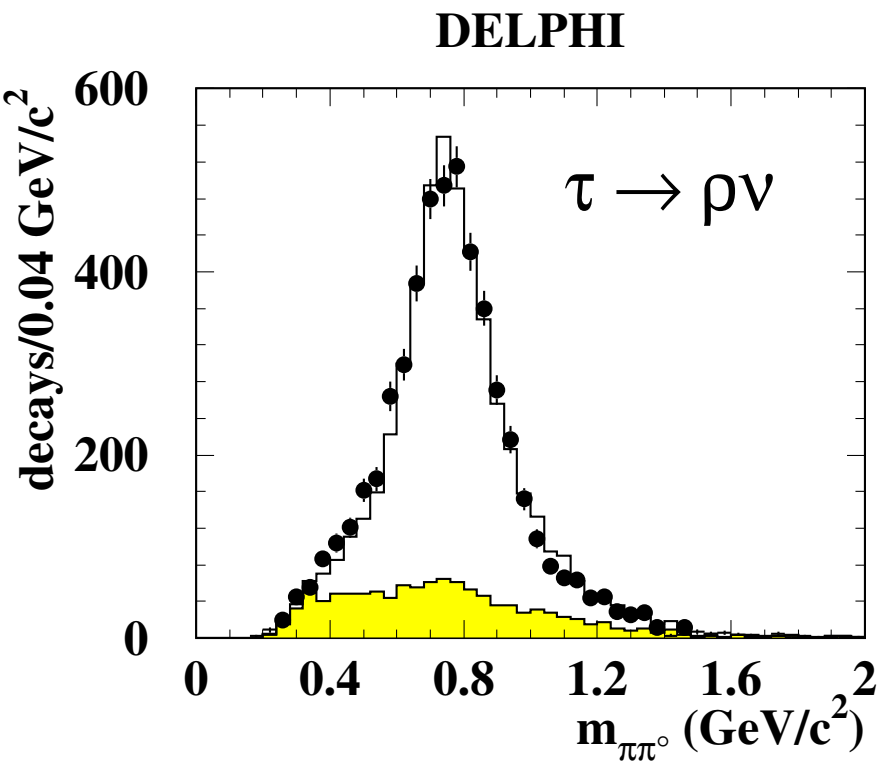

Figure 9: $\pi\pi^0$ invariant mass distribution for $\tau \to \rho\nu \to \pi\pi^0\nu$ candidate decays. The dots show the real data and the solid line simulated data. The hatched area is the background predicted by the simulation.

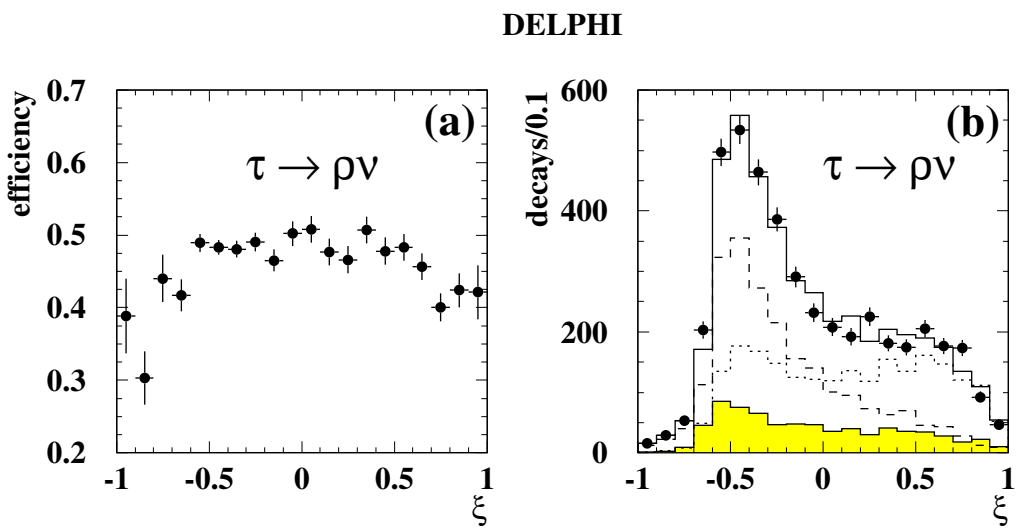

Figure 10: a) The selection efficiency determined from simulated data, as a function of ξ. b) The observed ξ spectrum of candidate $\tau \to \rho\nu$ decays with the same conventions as in Fig. 6.

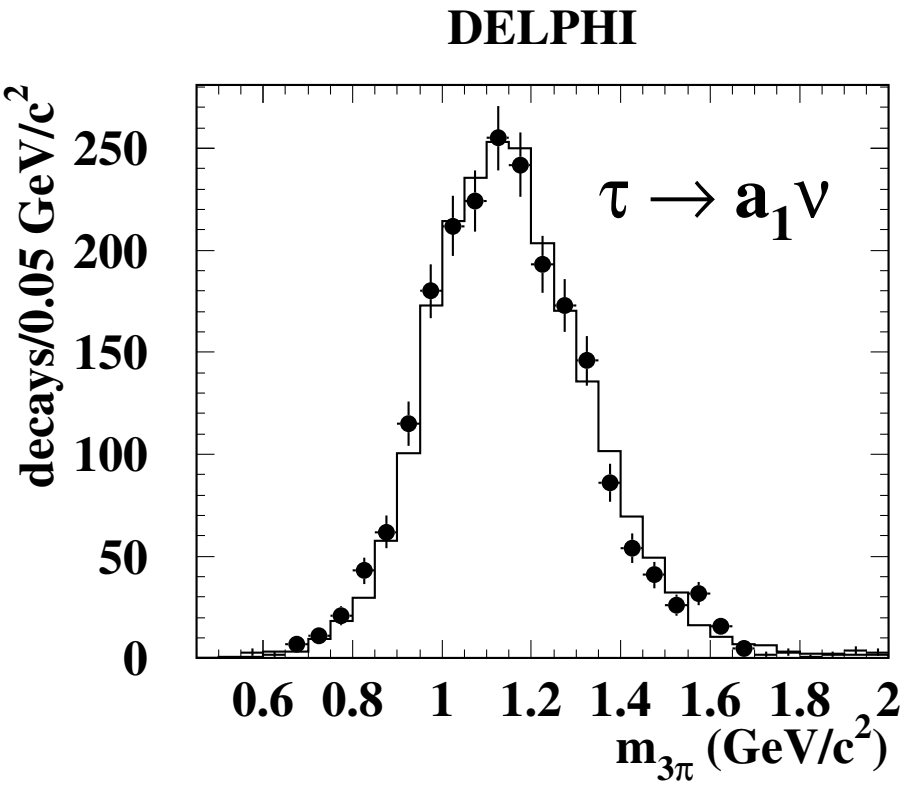

Figure 11: The 3π invariant mass spectrum from $\tau \to 3\pi^{\pm}\nu_{\tau}$ decays. The points are data and the histogram corresponds to simulated events generated with the mass and width obtained from a fit to the data.

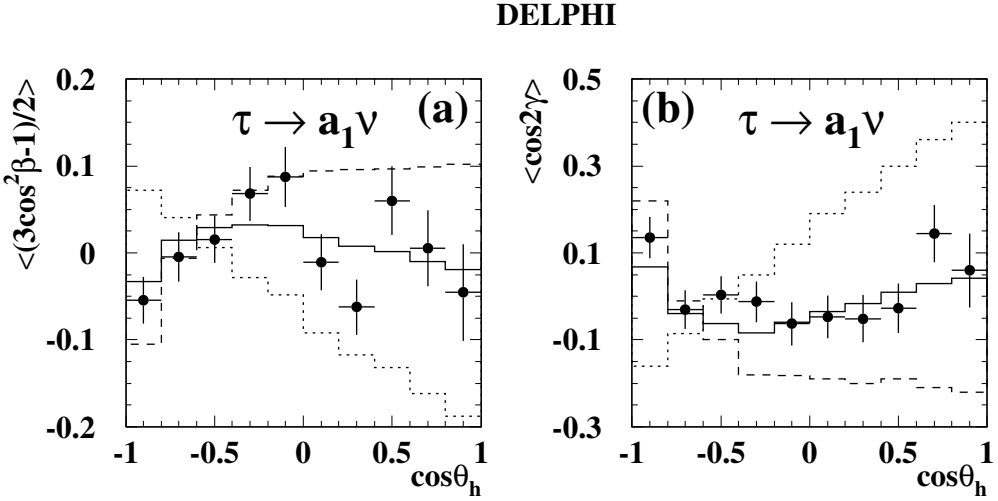

Figure 12: The two most sensitive moments in the polarisation fit of the $\tau \to \mathrm{a}_1\nu$ channel as a function of $\cos\theta_h$: a) $\langle(3\cos^2\beta - 1)/2\rangle$ and b) $\langle\cos 2\gamma\rangle$. The dots show the data and the solid line is simulated data with the fitted value of $\langle\mathcal{P}_\tau\rangle$. The dotted and dashed lines correspond to the positive and the negative polarisation distributions respectively.

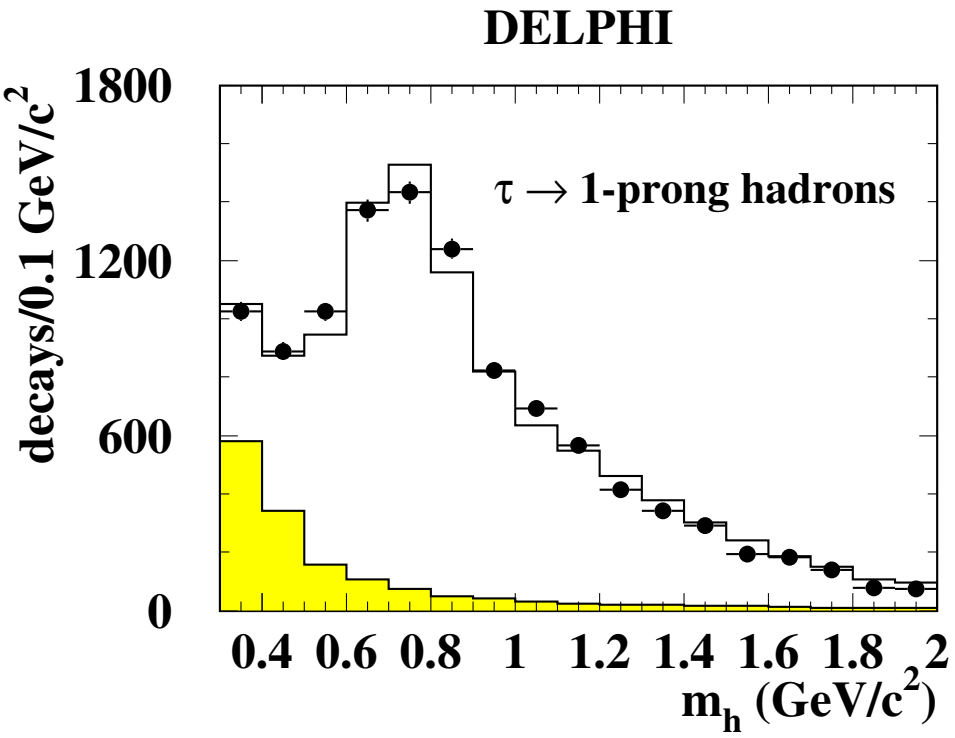

Figure 13: The observed invariant mass distribution for candidate events in the one-prong hadron inclusive analysis, before cuts to remove electrons. The pole at $m = m_\pi$ is not shown. The dots are data, the solid line is simulated data, and the hatched area is background.

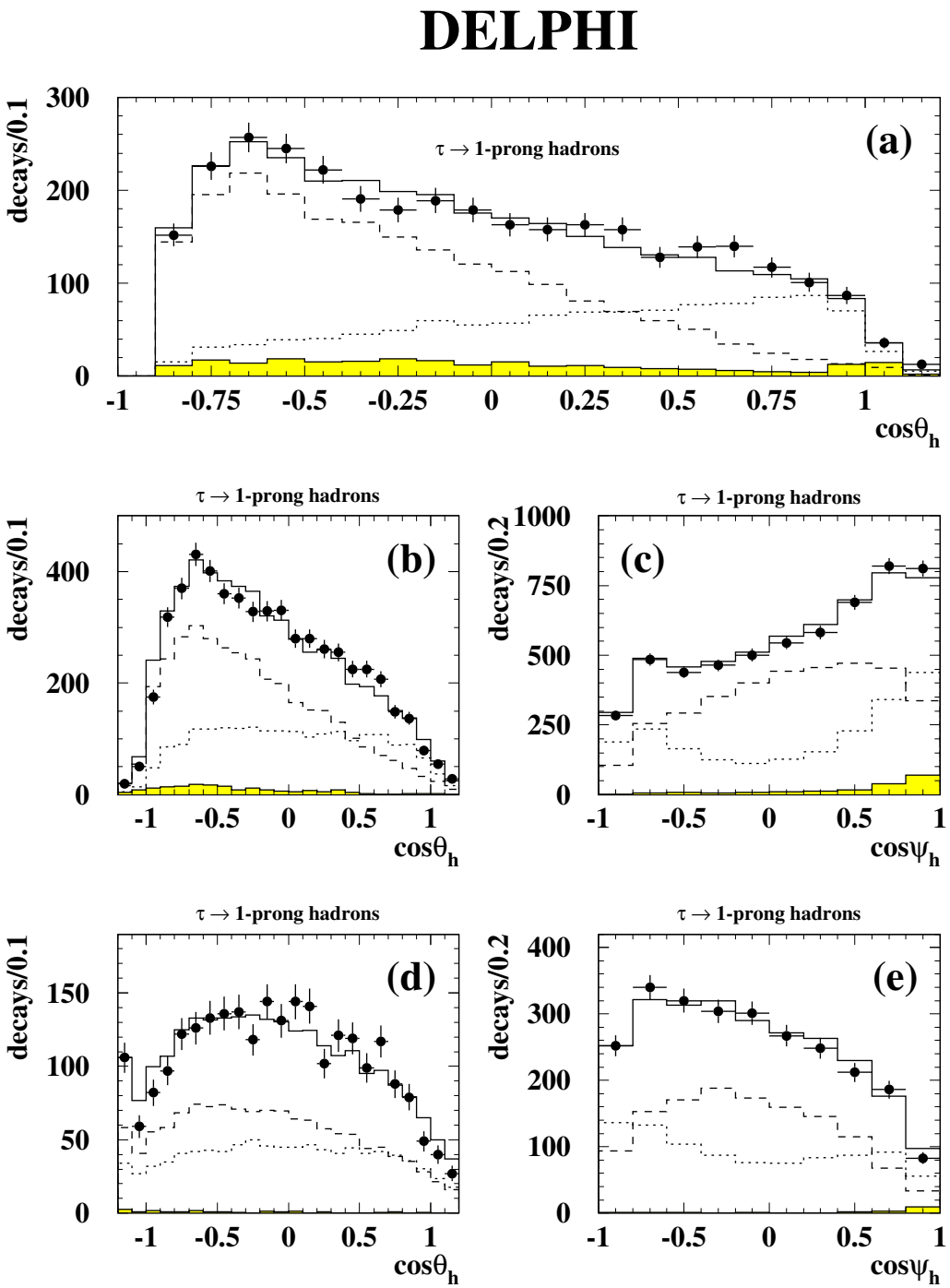

Figure 14: For the one-prong hadron inclusive analysis, the projections of the $\cos\theta_h$ vs $\cos\psi_h$ 2-dimensional distributions for the three invariant mass regions: a) $m_h < 0.3$ GeV/c^2; b) and c) 0.3 GeV/c^2 $< m_h <$ 0.9 GeV/c^2; d) and e) 0.9 GeV/c^2 $< m_h <$ 1.8 GeV/c^2; The dots are data and the solid line is simulated data for the fitted value of $\langle \mathcal{P}_\tau \rangle$. The hatched area is background and the dotted and dashed lines are the positive and negative polarisation contributions respectively.

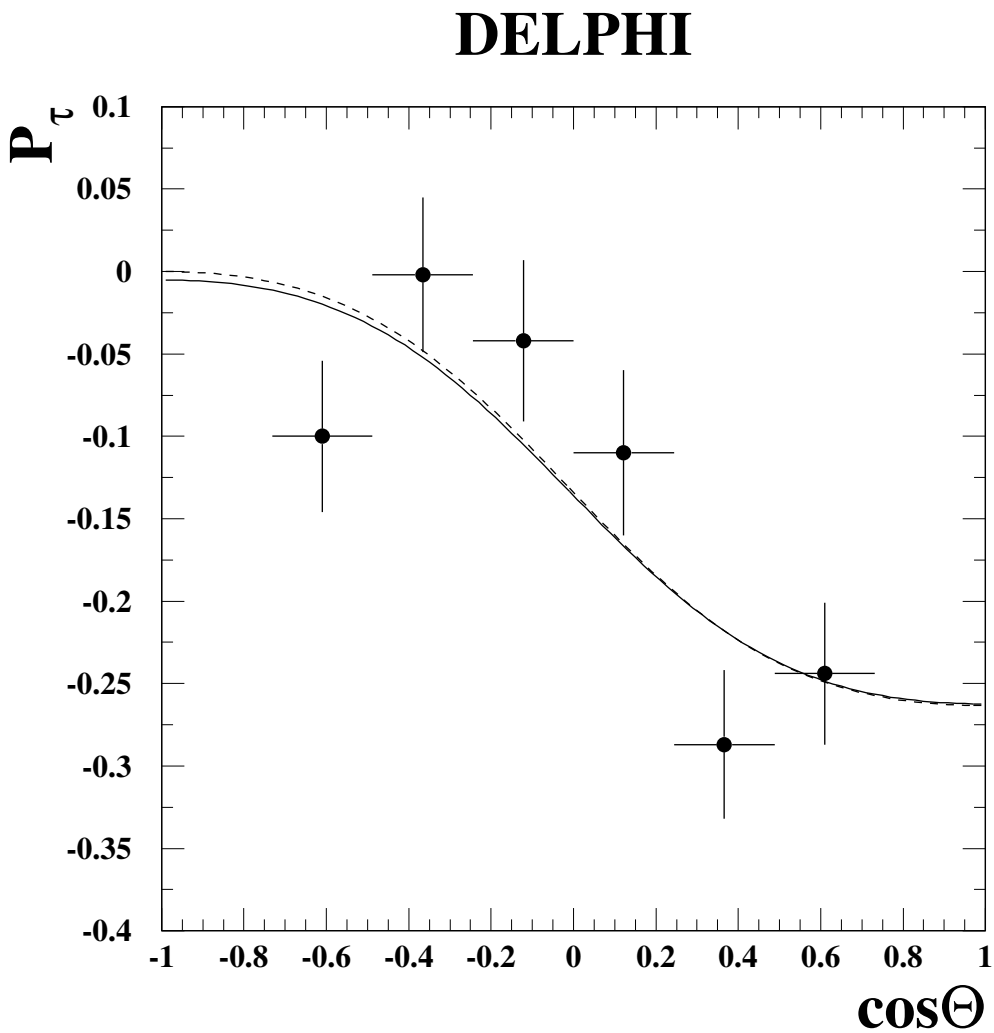

Figure 15: Data points show measured $\mathcal{P}_\tau$ as a function of cosΘ. The solid line represents the fit result without the assumption of universality, while the dashed line is the fit with universality assumed.